Stem Cell Reports
Article

ISSCR

OPEN ACCESS

Direct Conversion of Mouse Fibroblasts into Cholangiocyte Progenitor Cells

Kyung Tae Lim,[1,8] Jonghun Kim,[1,8] Seon In Hwang,[1,8] Ludi Zhang,[2] Heonjong Han,[3] Dasom Bae,[3] Kee-Pyo Kim,[4] Yi-Ping Hu,[5] Hans R. Schöler,[1,4] Insuk Lee,[3] Lijian Hui,[2] and Dong Wook Han[1,6,7,*]

[1]Department of Stem Cell Biology, School of Medicine, Konkuk University, 120 Neungdong-ro, Gwangjin-gu, Seoul 05029, Republic of Korea
[2]State Key Laboratory of Cell Biology, Institute of Biochemistry and Cell Biology, Shanghai Institutes for Biological Sciences, Chinese Academy of Sciences, Shanghai 200031, China
[3]Department of Biotechnology, College of Life Science and Biotechnology, Yonsei University, Seoul 04056, Republic of Korea
[4]Department of Cell and Developmental Biology, Max Planck Institute for Molecular Biomedicine, Röntgenstrasse 20, 48149 Münster, Germany
[5]Department of Cell Biology, Second Military Medical University, Shanghai 200433, China
[6]KU Open-Innovation Center, Institute of Biomedical Science & Technology, Konkuk University, 120 Neungdong-ro, Gwangjin-gu, Seoul 05029, Republic of Korea
[7]Department of Advanced Translational Medicine, School of Medicine, Konkuk University, 120 Neungdong-ro, Gwangjin-gu, Seoul 05029, Republic of Korea
[8]Co-first author
*Correspondence: dwhan@konkuk.ac.kr
https://doi.org/10.1016/j.stemcr.2018.03.002

SUMMARY

Disorders of the biliary epithelium, known as cholangiopathies, cause severe and irreversible liver diseases. The limited accessibility of bile duct precludes modeling of several cholangiocyte-mediated diseases. Therefore, novel approaches for obtaining functional cholangiocytes with high purity are needed. Previous work has shown that the combination of *Hnf1β* and *Foxa3* could directly convert mouse fibroblasts into bipotential hepatic stem cell-like cells, termed iHepSCs. However, the efficiency of converting fibroblasts into iHepSCs is low, and these iHepSCs exhibit extremely low differentiation potential into cholangiocytes, thus hindering the translation of iHepSCs to the clinic. Here, we describe that the expression of *Hnf1α* and *Foxa3* dramatically facilitates the robust generation of iHepSCs. Notably, prolonged *in vitro* culture of *Hnf1α*- and *Foxa3*-derived iHepSCs induces a Notch signaling-mediated secondary conversion into cholangiocyte progenitor-like cells that display dramatically enhanced differentiation capacity into mature cholangiocytes. Our study provides a robust two-step approach for obtaining cholangiocyte progenitor-like cells using defined factors.

INTRODUCTION

Cell therapy using hepatocytes has been highlighted as a promising treatment for repairing the irreversible liver diseases as an alternative to liver transplantation (Dhawan et al., 2010; Forbes et al., 2015). However, due to the limited accessibility and non-expandable nature of primary hepatocytes, a number of studies have attempted to generate hepatocyte-like cells from distinct types of stem cells, such as pluripotent stem cells (PSCs) (Hay et al., 2008; He et al., 2014; Si-Tayeb et al., 2010; Zhang et al., 2012). Indeed, hepatocyte-like cells generated from PSCs clearly share the key cellular features of primary hepatocytes (Hay et al., 2008; Si-Tayeb et al., 2010), but ethical and safety concerns abound on the use of PSC-derived hepatocyte-like cells in the clinic (Tang et al., 2011). To obviate the issues associated with using PSC-derived hepatocyte-like cells, recent studies directly generated hepatocyte-like cells, namely iHeps (induced hepatocyte-like cells), from both mouse and human somatic cells with defined factors without the cells having to first pass through a PSC state (Du et al., 2014; Huang et al., 2011, 2014; Kim et al., 2015; Lim et al., 2016; Sekiya and Suzuki, 2011).

Recent studies have demonstrated that the relatively small population of non-parenchymal cell types, such as cholangiocytes, plays also an important role in liver regeneration (Alvaro et al., 2007; Walter et al., 2014). Recently developed direct conversion technology has been applied for generating self-renewing and bipotential HepSCs, so-called induced hepatic stem-like cells (iHepSCs), using the defined factors *Hnf1β* and *Foxa3* (Yu et al., 2013). But prior to the translation of iHepSC technology to the clinic, a few issues need clear resolution. First, the final factor combination for iHepSC generation was determined without considering the actual conversion efficiency using authentic HepSC-specific markers. Second, the efficiency of converting somatic cells into iHepSCs is very low, less than 0.5%, and needs to be improved. Third, and most importantly, iHepSCs exhibit very low differentiation potential into mature cholangiocytes, which strongly necessitates further optimization of the combination of factors used for obtaining either iHepSCs with enhanced cholangiocyte differentiation potential or cholangiocyte progenitor cells (CPCs).

In the current study, we revisited the roles of several HepSC-specific candidate factors in reprogramming and found that the combination of *Hnf1α* and *Foxa3* dramatically facilitates the generation of iHepSCs that are transcriptionally closer to the endogenous hepatic progenitor cells than are iHepSCs from previous study. Moreover, the prolonged culture of *Hnf1α* and *Foxa3*-derived iHepSCs

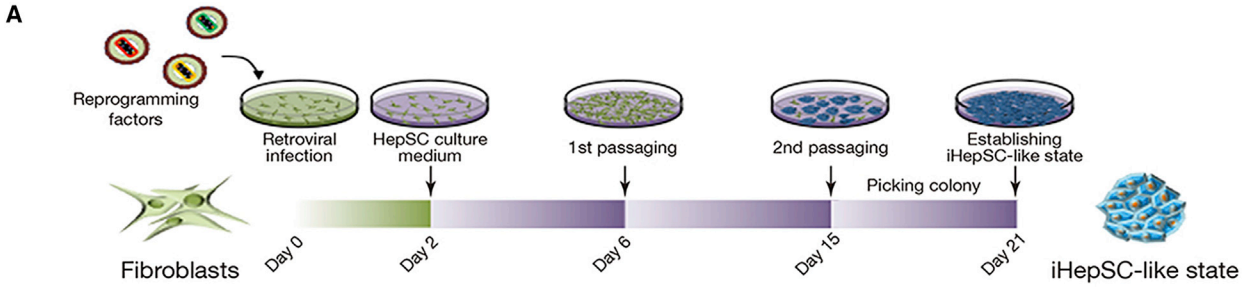

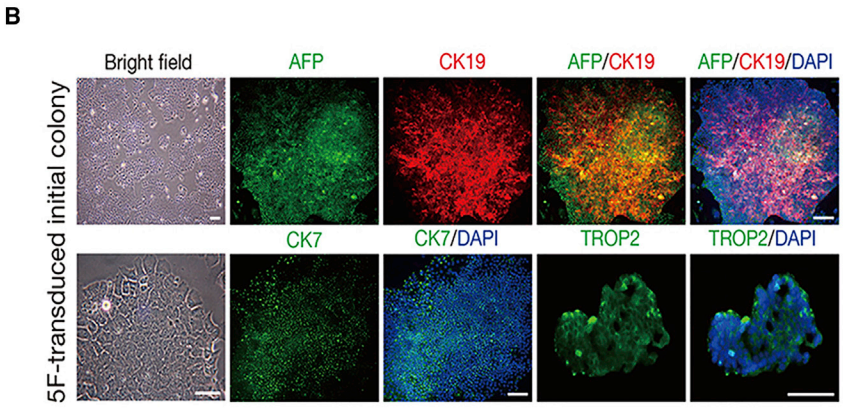

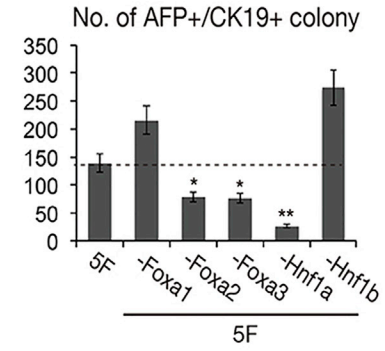

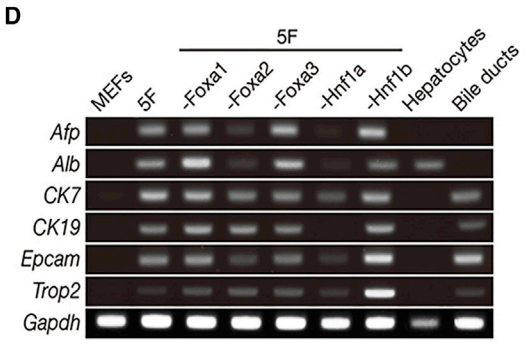

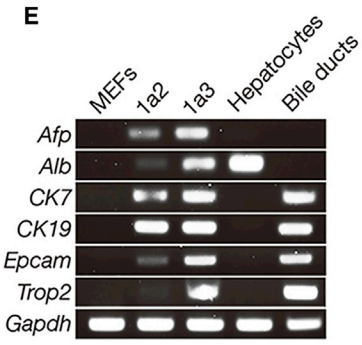

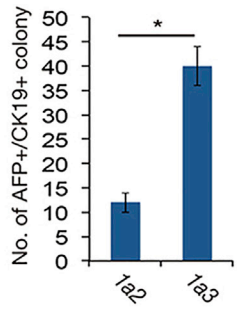

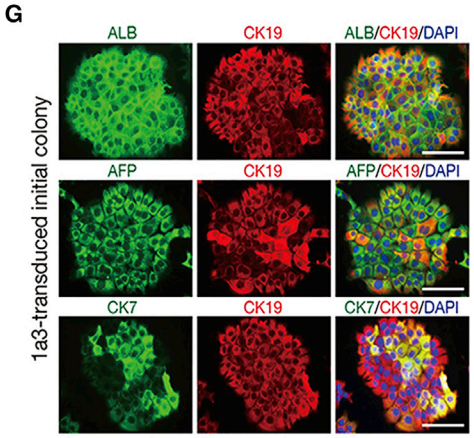

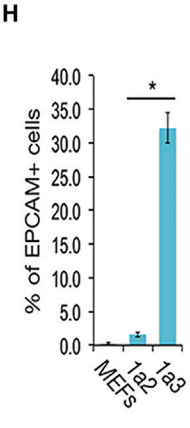

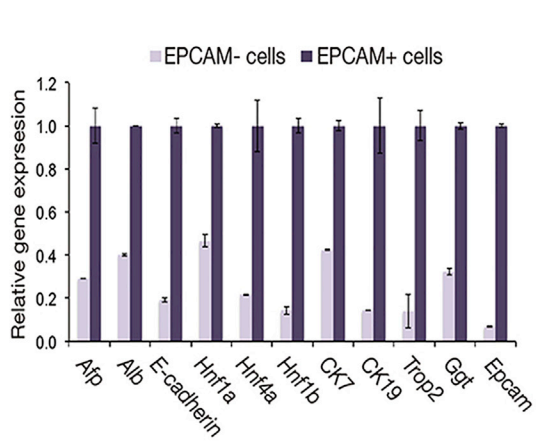

(legend on next page)

could induce further reprogramming that is mediated by Notch signaling into cholangiocyte progenitor-like cells, so-called induced CPCs (iCPCs), which display dramatically enhanced differentiation potential into mature cholangiocytes. Our study provides a strategy for generating iCPCs using defined factors.

RESULTS

Hnf1α and *Foxa3* Robustly Induce Hepatic Stemness in Fibroblasts

To define the combination of factors that is required for inducing either HepSC or CPC identities in somatic cells, we selected five candidate factors based on their roles in liver development (*Foxa1*, *Foxa2*, and *Hnf1β*) and regeneration (*Foxa3* and *Hnf1α*). Mouse embryonic fibroblasts (MEFs), which are devoid of epithelial cells, were transduced with all candidate factors as described previously (Lim et al., 2016) (Figure 1A). After 2 weeks of transduction, we observed the growth of epithelial colonies of a compact and three-dimensional (3D) shape that was morphologically distinct from that typical of iHep colonies (Figure S1A). Notably, a significant number of colonies expressed both the fetal hepatocyte marker α-fetoprotein (AFP) and the cholangiocyte marker cytokeratin 19 (CK19) (67.5% ± 13.5%; Figures 1B and 1C). Moreover, these colonies were strongly positive for other cholangiocyte and HepSC markers, such as CK7 and TROP2, respectively (Figure 1B). However, partially reprogrammed cells with epithelial morphology failed to activate both AFP and CK19 (Figure S1B), indicating that our unbiased approach could accurately measure the conversion efficiency. Taken together, the epithelial colonies that had emerged from the five factor-transduced MEFs might have a cellular identity similar to HepSCs and distinct from iHeps.

We next attempted to minimize the number of factors required for iHepSC conversion. For this, we removed the factors from the cocktail one by one and found that removing any of the three factors *Foxa2*, *Foxa3*, and *Hnf1α* drastically reduced the number of AFP$^+$/CK19$^+$ iHepSC colonies (Figure 1C). The removal of either *Hnf1β* or *Foxa1* did not negatively influence both iHepSC conversion and hepatic gene activation (Figures 1C and 1D). In contrast, iHepSCs generated in the absence of *Hnf1α* displayed poor activation of endogenous HepSC markers (Figure 1D). However, the gene expression pattern of iHepSCs generated in the absence of either *Foxa2* or *Foxa3* was comparable with that of iHepSCs generated with all five factors together (Figure 1D). Thus, we hypothesized that *Hnf1α* might play a key role in the transcriptional activation of the endogenous hepatic program and that *Foxa2* and *Foxa3* might rather play assistant roles that would enhance the conversion efficiency (Figures 1C and 1D). To test our hypothesis, we introduced *Hnf1α* with either *Foxa2* (1a2) or *Foxa3* (1a3) in MEFs. Interestingly, 1a3-transduced MEFs exhibited the more mature expression patterns of both cholangiocyte (*CK7* and *CK19*) and HepSC (*Epcam* and *Trop2*) markers (Figure 1E) with significantly higher numbers of AFP$^+$/CK19$^+$ iHepSC colonies (Figure 1F) than did 1a2-transduced MEFs. The majority of 1a3-derived iHepSC colonies were strongly double-positive for other hepatocyte and cholangiocyte markers (Figure 1G). Notably, 1a3-transduced MEFs produced a significantly higher number of EPCAM$^+$ cells strongly expressing hepatocyte-, cholangiocyte-, and HepSC-specific markers (Figures 1H and 1I). All the clonal lines derived from 1a3-transduced MEFs displayed the features typical of HepSCs as determined by a series of gene expression analyses (Figures S1C–S1E). Finally, iHepSCs could be generated from mouse adult tail-tip fibroblasts and were stably expanded for more than 10 passages without losing features typical of HepSCs (Figures S1F and S1G). Notably, three-factor (*Hnf1α*, *Foxa2*,

Figure 1. Direct Conversion of Fibroblasts into iHepSCs by *Hnf1α* and *Foxa3*

(A) Schematic depicting the procedure for the direct conversion of fibroblasts into iHepSCs.

(B) Immunofluorescence of iHepSC colony after 2 weeks of transducing all five transcription factors. Nuclei were stained with DAPI. Scale bars, 100 μm.

(C) The number of AFP$^+$/CK19$^+$ colonies was counted after 2 weeks of transduction. Data are presented as mean ± SD from three independent experiments. Two-tailed Student's t test: *$p < 0.05$, **$p < 0.01$.

(D and E) Expression patterns of hepatocyte-, cholangiocyte-, and HepSC-specific markers were analyzed by RT-PCR after transduction of MEFs with different combinations of factors.

(F) The number of AFP$^+$/CK19$^+$ colonies was counted on day 14 post transduction of MEFs with *Hnf1α* together with *Foxa2* (1a2) or *Foxa3* (1a3). Data are presented as mean ± SD from three independent experiments. Two-tailed Student's t test: *$p < 0.05$.

(G) Immunofluorescence of 1a3-transduced iHepSC colony. The nuclei were stained with DAPI. Scale bars, 100 μm.

(H) Percentage of EPCAM$^+$ cells was evaluated by flow cytometry 2 weeks after transduction of MEFs with either 1a2 or 1a3. MEFs, i.e., non-transduced cells, were used as a negative control. Data are presented as mean ± SD from three independent experiments. Two-tailed Student's t test: *$p < 0.05$.

(I) Expression of hepatocyte-, cholangiocyte-, and HepSC-specific markers in EPCAM$^+$ or EPCAM$^-$ cells was measured by qPCR. The levels were normalized to those of EPCAM$^+$ cells and are presented as mean ± SD from triplicate values.

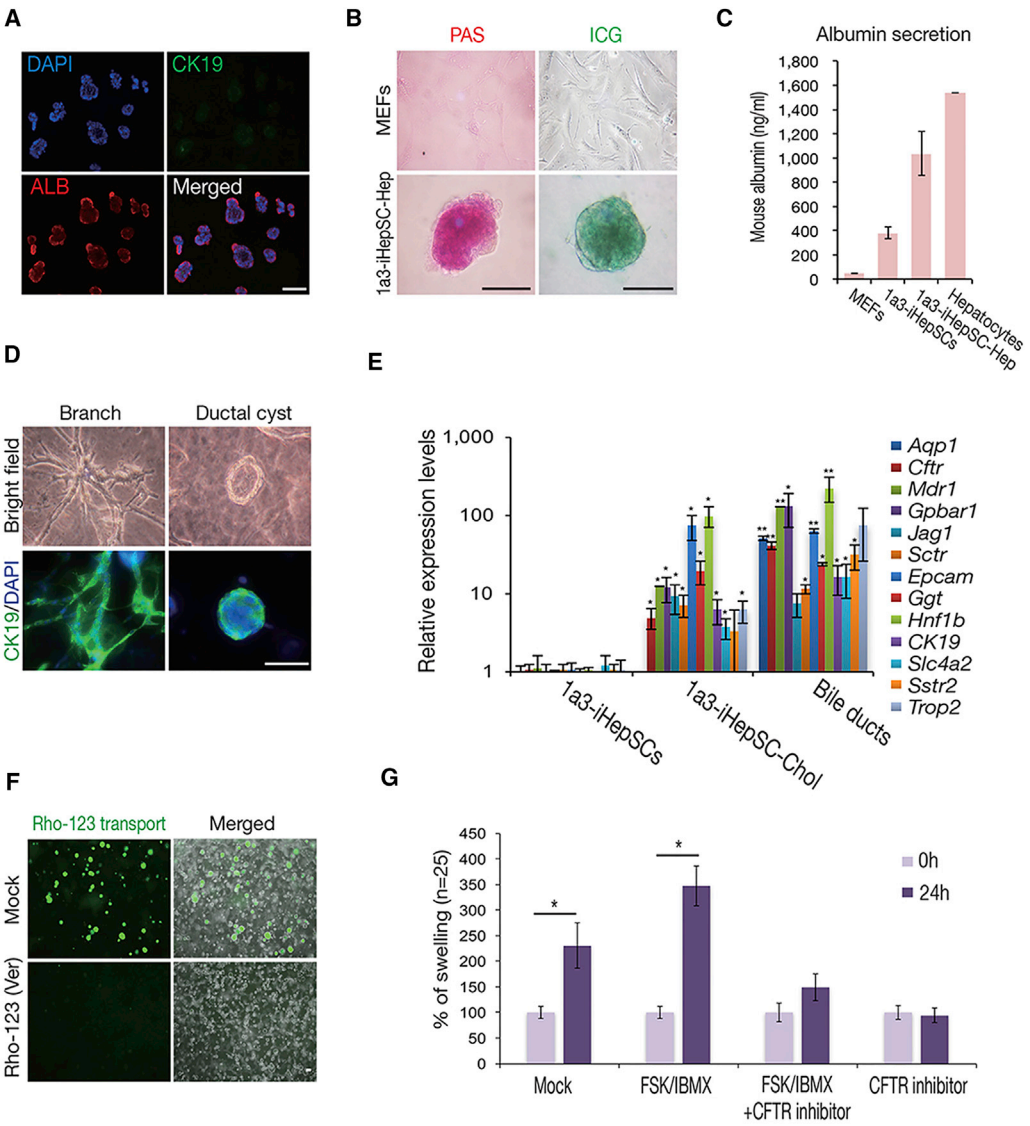

Figure 2. Differential Potential of 1a3-iHepSCs into Mature Hepatocytes and Cholangiocytes *In Vitro*

(A) Immunofluorescence of established 1a3-iHepSC-derived hepatocytes. The nuclei were stained with DAPI. Scale bar, 100 μm.

(B) *In vitro* functional analyses of 1a3-iHepSC–derived hepatocytes by periodic acid-Schiff (PAS) staining and indocyanine green (ICG) uptake assay. Scale bars, 100 μm.

(C) Serum albumin secreted from 1a3-iHepSC-derived hepatocytes was measured by ELISA. MEFs and primary hepatocytes were used as negative and positive controls, respectively. Data are presented as mean ± SD from triplicate values.

(D) Morphology of 1a3-iHepSC–derived cholangiocytes in branches and ductal cysts was analyzed under bright-field (upper panel) and immunofluorescence (lower panel) microscopy. Antibody directed against CK19 was used, and the nuclei were stained with DAPI. Scale bar, 100 μm.

(E) Expression of mature cholangiocyte markers was evaluated by qPCR upon cholangiocyte differentiation. All the values were normalized to those of undifferentiated 1a3-iHepSCs. Bile duct tissues were used as a positive control. Data are presented as mean ± SD of triplicate values from three individual cell lines. Two-tailed Student's t test: *$p < 0.05$, **$p < 0.01$.

(F) Transport of rhodamine-123 (Rho123) into the central lumen of a ductal cyst. Treatment with the MDR inhibitor verapamil (Ver) to block the transport activity of 1a3-iHepSC-derived ductal cysts. Scale bar, 100 μm.

(G) Quantification of degree of cyst swelling of 1a3-iHepSC–derived cholangiocytes after 24 hr of stimulation with forskolin (FSK) and IBMX in the absence or presence of the CFTR inhibitor $CFTR^{inh}$-172. The degree of swelling after 24 hr of stimulation was quantified based on the unstimulated cyst size. Five cysts in each group from three independent experiments were analyzed. Data are presented as mean ± SD. Paired t test: *$p < 0.05$.

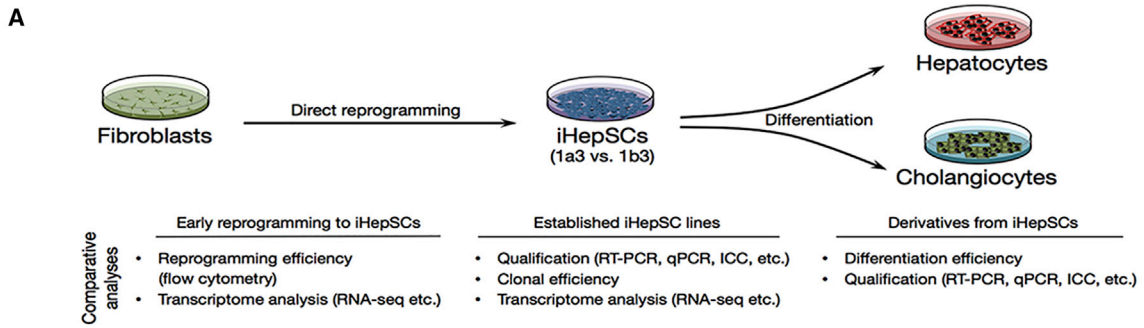

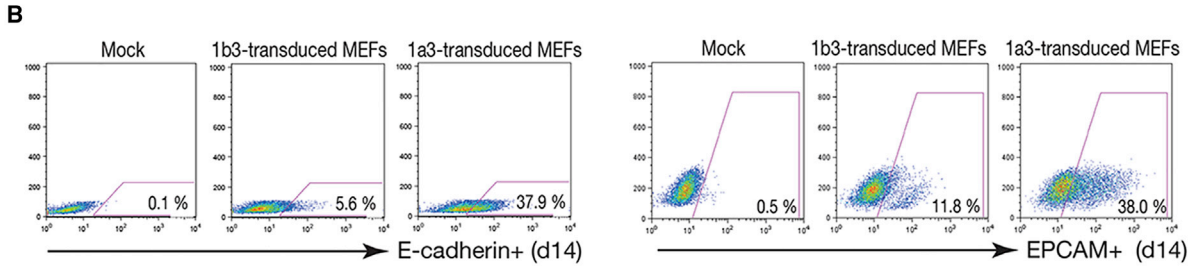

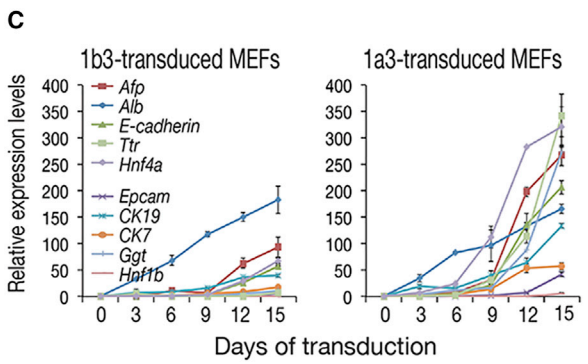

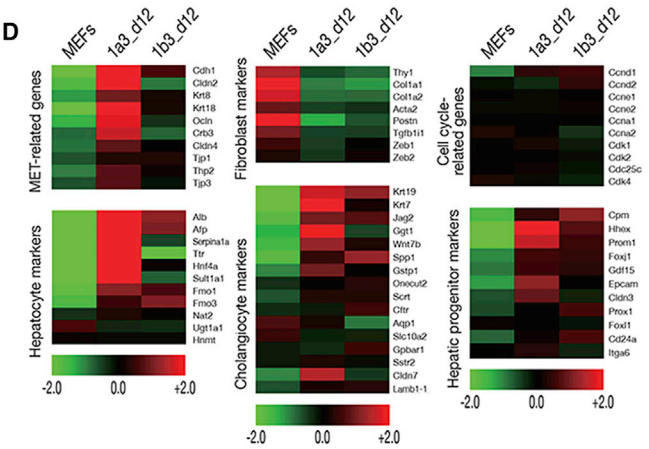

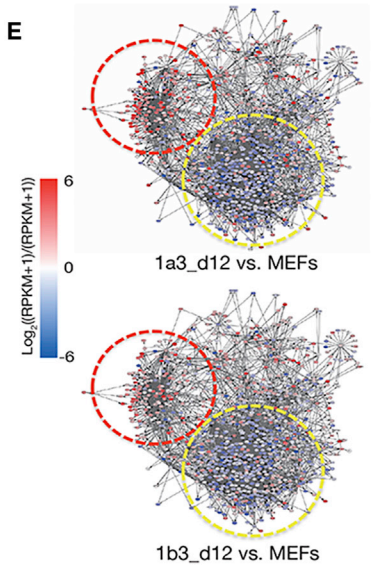

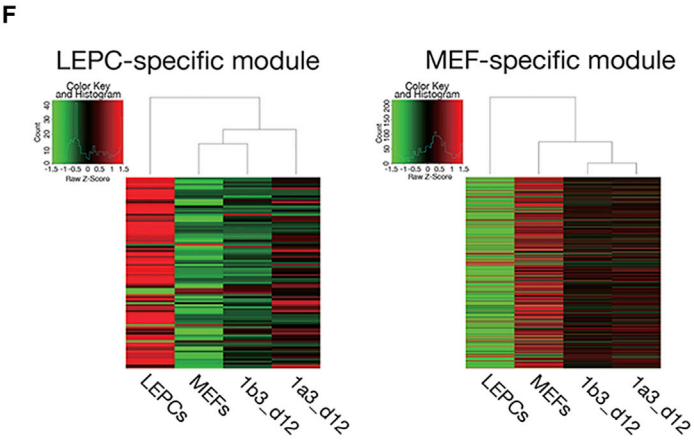

(legend on next page)

and *Foxa3*; 1a23) could not further enhance reprogramming efficiency compared with 1a3 (Figure S1H). Taken together, our data clearly show that 1a3 is the best combination for a robust induction of hepatic stemness on somatic cells but is not enough for inducing a CPC cell identity.

1a3-iHepSCs Can Differentiate into Mature Hepatocytes and Cholangiocytes *In Vitro*

We next assessed the *in vitro* differentiation potential of 1a3-derived iHepSCs (hereafter referred to as 1a3-iHepSCs) to determine whether they had acquired hepatic stemness. Within 24 hr of hepatic differentiation (Li et al., 2006; Yu et al., 2013), aggregates typical of differentiated cells were readily observed (Figure S2A). After 7 days, we were able to identify mature aggregates with strong activation of albumin (ALB) and complete inactivation of CK19 (Figure 2A). RT-PCR analysis also showed that the expression of hepatocyte markers was strongly upregulated, whereas both cholangiocyte and HepSC markers were dramatically suppressed (Figure S2B). Moreover, 1a3-iHepSCs were found to display glycogen storage, xenobiotic metabolic activity, and albumin secretion upon hepatic differentiation, indicating that they have the potential to differentiate into mature hepatocytes *in vitro* (Figures 2B and 2C).

After 7 days of differentiation into cholangiocytes (Li et al., 2010), 1a3-iHepSCs had differentiated into $CK19^+$ cholangiocytes that exhibited a typical branching structure (Figure 2D, left). Under 3D differentiation conditions containing 40% Matrigel (Tanimizu et al., 2007), we observed $CK19^+$ mature cystic structures (Figure 2D, right). The cysts strongly expressed cholangiocyte-associated genes (Figure 2E) and exhibited apicobasal polarity as shown by the localization of F-actin in the inner layer of the lumen (Figure S2C), demonstrating that cholangiocytes that had differentiated from 1a3-iHepSCs share molecular and structural characteristics with primary cholangiocytes. A major physiological function of cholangiocytes is the secretion of substances such as water and ions for modulating bile composition, and this process is mediated by transmembrane channel proteins such as multidrug resistance protein 1 (MDR1) and cystic fibrosis transmembrane regulator (CFTR). Thus, we examined the transporter activity of MDR1 in the cholangiocytes derived from 1a3-iHepSCs by evaluating the efflux of rhodamine-123 (Rho123), and found that the cholangiocytes could transport Rho123 into the luminal space (Figure S2D). However, in the presence of the MDR1 inhibitor verapamil, Rho123 did not accumulate in the lumen, indicating that the differentiated cholangiocytes in cysts behave like their *in vivo* counterpart (Figure 2F). We also performed a forskolin-induced swelling assay to monitor CFTR-mediated fluid transport and cyst swelling in the cholangiocytes. After 24 hr of forskolin treatment, the size of the cysts had increased by 3.31 ± 0.44-fold (Figures 2G and S2E). In contrast, the forskolin/IBMX (3-isobutyl-1-methylxanthine)-induced cyst swelling was abolished in the presence of $CFTR^{inh}$-172, a CFTR inhibitor, showing that the size of the cysts that had differentiated from 1a3-iHepSCs is regulated by CFTR, as in *in vivo* cholangiocytes (Figure 2G). Notably, iHepSCs from adult tail-tip fibroblasts also differentiated into both hepatocytes and cholangiocytes (Figures S2F and S2G). Taken together, our data clearly indicate that 1a3-iHepSCs possess an *in vitro* differentiation potential into both functionally mature hepatocytes and cholangiocytes.

Hnf1α Plays a Critical Role in the Induction Phase of Hepatic Stemness Acquisition

As the previous study (Yu et al., 2013) had used *Hnf1β* and *Foxa3* (1b3) for converting fibroblasts into iHepSCs, we decided to compare the roles of the two reprogramming cocktails 1a3 and 1b3 during the induction phase of hepatic stemness acquisition (Figure 3A). In line with our

Figure 3. *Hnf1α* Plays a Critical Role in the Induction Phase of Hepatic Stemness Acquisition

(A) Schematic comparing the direct conversion process of fibroblasts into iHepSCs driven by *Foxa3* together with *Hnf1α* (1a3) or *Hnf1β* (1b3).

(B) Conversion efficiency (%) into iHepSCs from the MEFs transduced with either 1a3 or 1b3 was determined by flow-cytometric analysis using an antibody directed against E-cadherin (left) or EPCAM (right) on day 14 of transduction.

(C) Expression of hepatocyte-, cholangiocyte-, and HepSC-specific markers was analyzed by qPCR in a time course manner after transduction of MEFs with each reprogramming cocktail. The levels were normalized to those of MEFs and are presented as mean ± SD of triplicate values.

(D) Heatmaps representing the expression patterns of markers related to mesenchymal-epithelial transition (MET) process, fibroblasts, cell cycle, hepatocytes, cholangiocytes, and hepatic progenitors after 12 days of introducing 1a3 or 1b3 into MEFs. Color bar at the bottom indicates gene expression in $\log_2$ scale. Red and green colors represent higher and lower expression levels, respectively.

(E) TRNs in the MEFs after 12 days of transducing MEFs with 1a3 or 1b3. Subnetwork modules were extracted using DEGs between LEPCs and MEFs by CellNet. Yellow and red dashed circles represent MEF- and LEPC-specific modules, respectively.

(F) Heatmaps describing gene expression profiles in LEPC- and MEF-specific modules in MEFs 12 days post infection with 1a3 or 1b3. Hierarchical clustering analysis based on the gene expression profiles from the heatmap is shown at the top. MEFs and LEPCs were used as negative and positive controls, respectively.

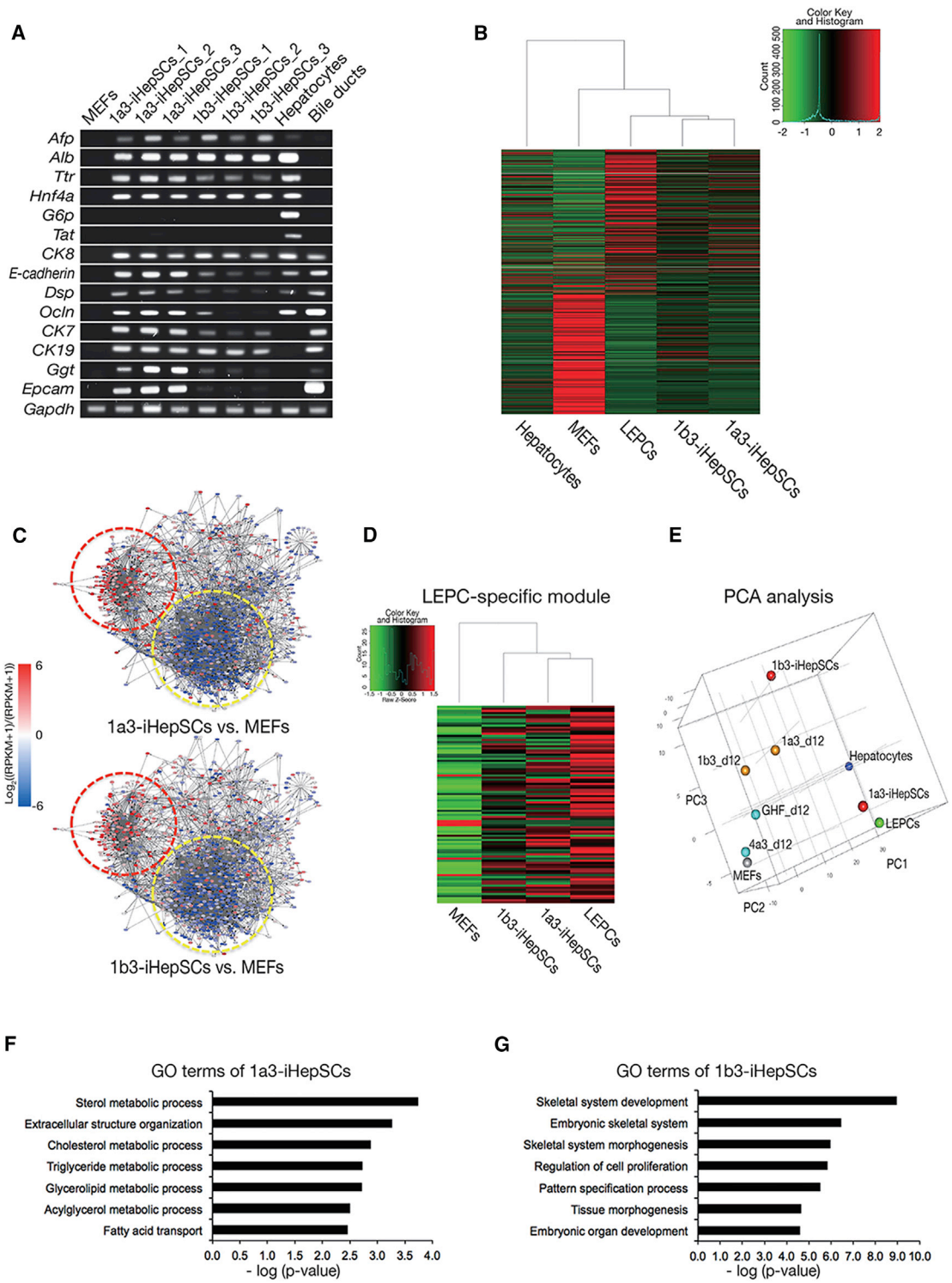

Figure 4. 1a3-iHepSCs Are Transcriptionally Closer Than 1b3-iHepSCs to LEPCs

(A) RT-PCR analysis comparing the expression pattern of hepatocyte-, cholangiocyte-, and HepSC-specific markers in three independent clonal lines from 1a3- and 1b3-iHepSCs, which were generated by fluorescence-activated cell sorting with EPCAM.

(B) Heatmap analysis describing whole-genome expression profiles of 1a3- and 1b3-iHepSCs at passage 10. Hierarchical clustering analysis based on the expression profiles from the heatmap is depicted at the top. MEFs and LEPCs were used as negative and positive controls, respectively.

(legend continued on next page)

screening assay results (Figure 1), 1a3-transduced MEFs produced significantly increased numbers of either E-cadherin$^+$ or EPCAM$^+$ populations compared with the 1b3-transduced MEFs (Figure 3B). This increased yield of 1a3 was due to neither distinct transduction levels of individual transgenes nor distinct proliferation rates of the MEFs transduced with distinct combinations of factors (Figures S3A and S3B). Notably, 1a3-transduced MEFs exhibited dramatically accelerated conversion kinetics toward a HepSC state, as evidenced by the enhanced activation of genes associated with hepatic stemness compared with 1b3-transduced MEFs (Figures 3C, 3D, and S3C). Taken together, these data suggest that a conversion cocktail 1a3 is more potent than 1b3 for the robust induction of hepatic stemness.

To explore the mechanism underlying 1a3-mediated enhanced iHepSC generation, we monitored the early transcriptional changes taking place following the introduction of 1a3 or 1b3 to the cells. Whole-genome transcription analysis revealed that a similar number of genes was either up- or downregulated (Figure S3D), and that both combinations activated similar pathways involved in various metabolic functions of the liver (Figure S3E). Despite this high similarity (Figure S3F), we found that 441 and 357 genes were highly enriched in 1a3- and 1b3-transduced MEFs, respectively (Figure S3G). Gene ontology (GO) analysis of differentially expressed genes (DEGs) from 1a3- and 1b3-transduced MEFs (1a3-DEGs and 1b3-DEGs) show that various metabolic processes were highly ranked in 1a3-DEGs, whereas the genes involved in cell adhesion and neuronal development were top-ranked in 1b3-DEGs (Figure S3H). These data underscore the notion that 1b3 could not sufficiently activate the HepSC program and has off-target effects, activating genes associated with ectoderm lineage.

We next investigated the transcriptional signatures of 1a3-and 1b3-transduced MEFs by comparing the cells' transcriptional regulatory network (TRN). To this end, we employed CellNet (Cahan et al., 2014), a computational network biology platform providing a comprehensive description of transcriptional networks constructed by numerous interactions among highly ranked transcription factors. We first generated a HepSC-TRN using both mouse liver epithelial progenitor cells (LEPCs)-specific DEGs (Li et al., 2006) and MEF-specific DEGs (Figure S3H). We found two major distinct subnetwork modules in the HepSC-TRN that are specific to LEPCs and MEFs, respectively (Figures S3I and S3J). To evaluate the early reprogramming status of both 1a3- and 1b3-transduced MEFs, we applied the DEGs (1a3 versus MEFs and 1b3 versus MEFs) on the HepSC-TRN (Figure 3E). In line with our kinetic analysis results (Figures 3C and 3D), 1a3-transduced MEFs displayed faster activation of genes involved in the LEPC-specific module compared with 1b3-transduced MEFs (Figure 3F). These data support the notion that *Hnf1α* is the authentic driving force for inducing hepatic stemness.

1a3-iHepSCs Are Transcriptionally Closer Than 1b3-iHepSCs to LEPCs

To compare the molecular and cellular characteristics of the established 1a3-iHepSCs with those of 1b3-iHepSCs, we generated three clonal iHepSC lines from each combination. During clonal expansion, we were unable to observe any significant difference in the proliferation rate and clonal efficiency of the resultant iHepSCs, indicating that the self-renewal capacities of both 1a3- and 1b3-iHepSCs are comparable (Figures S4A and S4B). Notably, the majority of stem cell markers were strongly activated in all 1a3-iHepSC clones, whereas some epithelial and HepSC markers were relatively less activated in most 1b3-iHepSC lines (Figure 4A). Heatmap analysis also showed that 1a3-iHepSCs displayed the relatively well-reprogrammed pattern of gene transcription compared with the expression pattern of 1b3-iHepSCs, although these cells clustered together (Figure 4B). Particularly, the fibroblast-specific transcriptional signature was largely maintained in the established 1b3-iHepSCs but nearly erased in 1a3-iHepSCs (Figure 4B), indicating that *Hnf1α* plays a critical role not only in the induction phase but also in the maturation phase of the process of acquiring hepatic stemness.

We also performed TRN analysis by applying both the 1a3- and 1b3-specific DEGs defined from the established iHepSC lines onto the HepSC-TRN (Figure 4C). Consistent with our expression profiling (Figures 4A and 4B), the expression levels of genes associated with LEPC-specific modules were significantly higher in 1a3-iHepSCs than in 1b3-iHepSCs, resulting in the relatively closer clustering of LEPCs and 1a3-iHepSCs (Figure 4D). Principal component analysis also showed that the expression pattern of the LEPC-specific module in 1a3-iHepSCs is very similar to that in LEPCs (Figure 4E). To our surprise, GO analysis showed that 1a3-specific DEGs were all associated with typical hepatic features, such as distinct metabolic processes (Figure 4F). However, non-hepatic events were highly ranked in 1b3-DEGs (Figure 4G), supporting the notion that 1b3 activates subsets of genes that do not

(C) TRNs in 1a3- and 1b3-iHepSCs. Yellow and red dashed circles represent MEF- and LEPC-specific modules, respectively.
(D and E) Heatmap (D) and PCA (E) describing the gene expression profiles of the LEPC-specific module in iHepSCs. Hierarchical clustering results are displayed on top of the heatmap. MEFs and LEPCs were used as negative and positive controls, respectively.
(F and G) GO enrichment analysis of each iHepSC-specific DEGs.

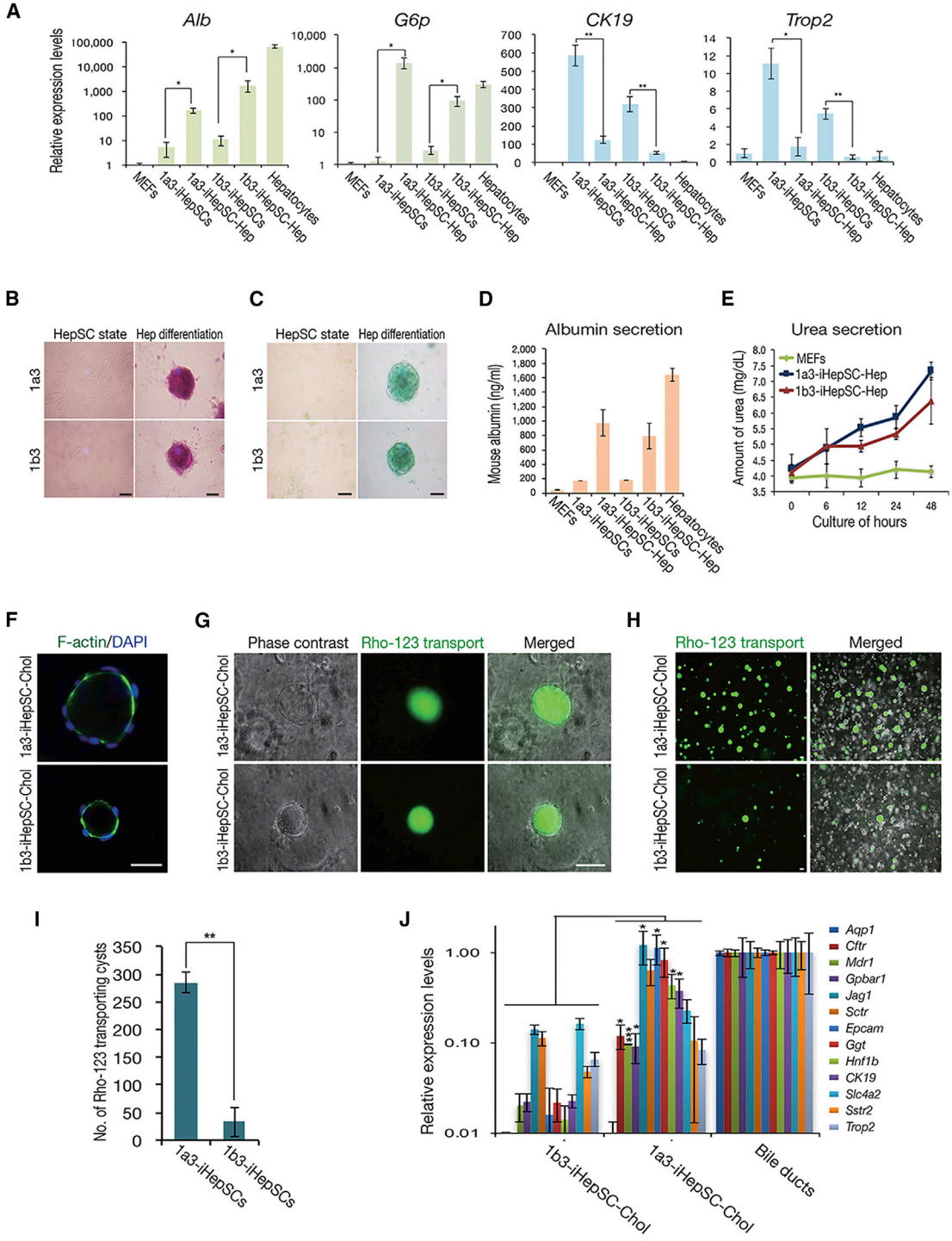

Figure 5. 1a3-iHepSCs Exhibit Enhanced Differentiation Potential into Cholangiocytes

(A) Expression of hepatocyte- and cholangiocyte-specific markers was analyzed by qPCR after 7 days of differentiation of iHepSCs. All the values were normalized to those of MEFs and are presented as mean ± SD of triplicate values from three biological replicates. Paired t test: *$p < 0.05$, **$p < 0.01$.

(B and C) *In vitro* functional analyses of iHepSC-derived hepatocytes by PAS staining (B) and ICG uptake assay (C). Scale bars, 100 μm.

(D and E) Comparison of secretion levels of serum albumin (D) and urea (E) from iHepSC-derived hepatocytes. MEFs and primary hepatocytes were used as negative and positive controls, respectively. Data are presented as mean ± SD of triplicate values.

(legend continued on next page)

belong to the hepatic lineage. Taken together, our data indicate that *Hnf1α* is indeed a master factor for inducing hepatic stemness.

Hnf1a Dramatically Enhances *In Vitro* Differentiation Potential of iHepSCs into Cholangiocytes

To investigate the effect of *Hnf1α* and *Hnf1β* on the functionality of iHepSCs, we compared the *in vitro* differentiation potential of the two iHepSC lines. Following 7 days of differentiation into hepatocytes, both iHepSC lines had formed typical aggregates and exhibited increased expression of mature hepatic genes but reduced expression of both cholangiocyte- and stem cell-specific markers (Figures 5A and S5A–S5D). Moreover, the genes associated with drug transport activity as well as the CYP450 genes were significantly increased to a similar extent (Figures 5E and 5F). The additional set of *in vitro* functional studies clearly suggests that the iHepSC lines from two distinct combinations are comparable in their hepatic differentiation capacity (Figures 5B–5E).

Next, we compared the differentiation potential of these two iHepSC lines into cholangiocytes. Although both 1a3- and 1b3-iHepSCs had formed cysts with typical apicobasal polarity under the 3D culture conditions (Figure 5F), their differentiation efficiency into cholangiocytes was dramatically different (Figures 5G and 5H). Indeed, 1a3-iHepSCs exhibited significantly increased numbers of Rho123-transporting mature cysts (8.6-fold higher) compared with 1b3-iHepSCs (Figure 5I). Furthermore, 1a3-iHepSC-derived cholangiocytes strongly expressed cholangiocyte markers to the level similar to that of bile duct tissues (Figure 5J). However, 1b3-iHepSC-derived cholangiocytes displayed relatively weak or no expression of those markers (Figure 5J). These data indicate that *Hnf1α* plays a crucial role as a determinant of hepatic stemness, resulting in the generation of iHepSCs with a dramatically enhanced cholangiocyte differentiation potential.

Notch Signaling-Mediated Secondary Conversion into Cholangiocyte Progenitor-like Cells

Interestingly, 1a3-iHepSCs from different passages (P10 and P30) displayed distinct differentiation efficiency toward mature cholangiocytes (Figure S6A). In contrast, their hepatic differentiation was dramatically reduced upon further passaging, and completely abolished in 1a3-iHepSCs from P30 (Figure S6B). To understand these distinct passage-dependent differentiation patterns of 1a3-iHepSCs toward cholangiocytes and hepatocytes, we determined the expression levels of hepatocyte and cholangiocyte markers. Although 1a3-iHepSCs from later passages (P20 and P30) displayed dramatically reduced levels of hepatocyte markers (Figures 6A and 6B), expression levels of cholangiocyte markers including *CK19*, *Aqp1*, *Cftr*, *Ggt*, and *Hnf β* were stably maintained or further enhanced even after long-term passaging (Figures 6A and S6C), indicating that prolonged *in vitro* culture could induce further commitment of 1a3-iHepSCs into iCPCs, which predominantly differentiate into mature cholangiocytes (Figures S6A and S6B). However, 1b3-iHepSCs maintained their hepatic stemness even after long-term culture (Figure 6A), suggesting that the secondary conversion of iHepSCs into iCPCs is mediated by 1a3 but not 1b3. This unique property of 1a3-iHepSCs offers a two-step strategy for generating iCPCs.

Recent studies have described Notch signaling-mediated differentiation of human PSCs into CPCs or mature cholangiocytes (Geisler et al., 2008; Ogawa et al., 2015; Sampaziotis et al., 2015). Thus we next investigated whether the secondary conversion of 1a3-iHepSCs into iCPCs is also governed by Notch signaling. As a result, we found that the expression levels of Notch and its targets (*Notch2*, *Jag1*, and *Hes1*) were increased upon serial passaging of 1a3-iHepSCs (Figure S6C). However, the expression levels of all the hepatic markers were stably maintained in 1a3-iHepSCs in the presence of DAPT, a γ-secretase inhibitor that blocks Notch signaling *in vitro* (Figures 6C–6E). Furthermore, the differentiation of 1a3-iCPCs (at P20) into mature cholangiocytes was completely blocked by DAPT treatment (Figures S6D–S6F). Taken together, our data indicate that the secondary conversion process of iHepSCs into iCPCs as well as the unipotential differentiation potential of iCPCs into mature cholangiocytes are determined by Notch signaling (Figure 6F).

To further investigate the *in vivo* functionality of 1a3-iCPCs, we used 3,5-diethoxycarbonyl-1,4-dihydrocollidine (DDC)-fed mice, a well-known model for activation of liver progenitor cells and bile duct proliferation (Preisegger et al., 1999), which allow for the spontaneous differentiation of

(F) Immunostaining images of F-actin in iHepSC-derived ductal cysts. Nuclei were stained with DAPI. Scale bars, 100 μm.
(G) Transport of Rho123 into the central lumen of a ductal cyst derived from iHepSCs. Scale bars, 100 μm.
(H and I) Image representation (H) and number (I) of Rho123-transporting cysts in the culture dish after 7 days of differentiation of iHepSCs. Three biological replicates of iHepSCs at passage 10 were used for the analysis. Data are presented as mean ± SD from three different experiments. Two-tailed Student's t test: $^{**}p < 0.01$. Scale bars, 100 μm.
(J) Expression of genes related to functional cholangiocytes was analyzed by qPCR. All the values were normalized to those of bile duct tissues as a positive control and are presented as mean ± SD of triplicate values from three biological replicates. Two-tailed Student's t test: $^{*}p < 0.05$, $^{***}p < 0.001$.

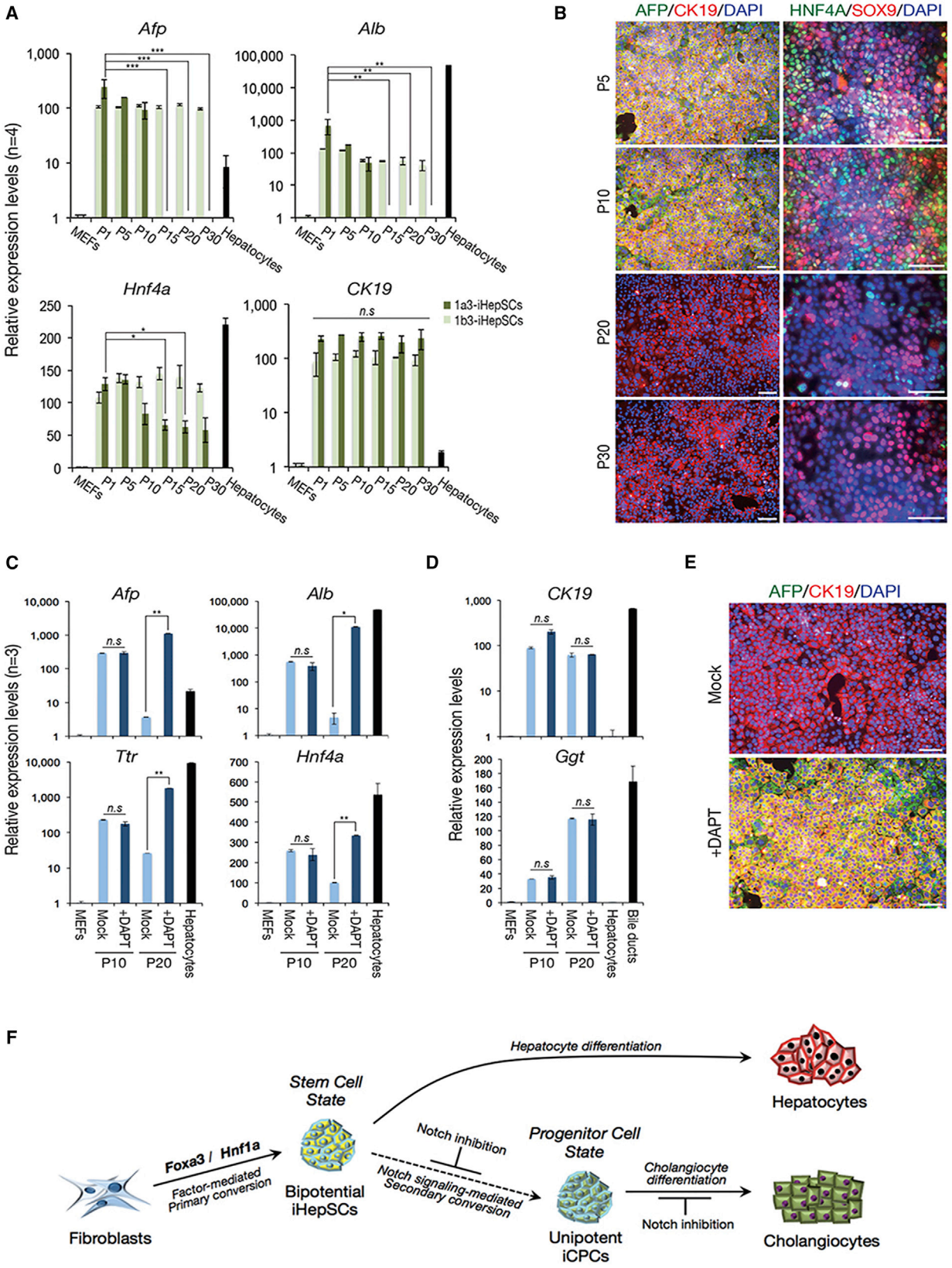

(legend on next page)

liver progenitor cells into cholangiocytes. 1×10^6 GFP-labeled 1a3-iCPCs (P20) with normal karyotype (Figure S7A) were transplanted into DDC-fed mice via intrasplenic injection. After 4 weeks of transplantation, the 1a3-iCPCs had not only incorporated into pre-existing bile ducts but also newly formed a significant number of GFP^+ ductal structures through bile ductular proliferation without forming tumor (Figures 7A and S7B). However, only a few GFP^+ ductal structures were observed in the liver sections of mice transplanted with 1b3-iHepSCs that had been maintained under the same culture conditions as the 1a3-iCPCs (Figure 7A). We compared the differentiation efficiency of both cell lines by counting the number of GFP^+ cholangiocytes per total number of cholangiocytes. The number of GFP^+ ductal structures derived from 1a3-iCPCs was significantly higher than that from 1b3-iHepSCs (Figure 7B), although the *in vivo* hepatic differentiation potential of 1b3-iHepSCs overwhelmingly exceeds that of 1a3-iCPCs (Figures S7C and S7D). Furthermore, a larger number of most GFP^+ 1a3-iCPC-derived cells strongly expressed CK19 and the functional cholangiocyte-specific marker osteopontin (OPN), compared with 1b3-iHepSC-derived cells (Figures 7C–7F). Collectively, these results clearly demonstrate that iCPCs that had converted from 1a3-iHepSCs via Notch signaling pathway are functionally mature.

DISCUSSION

To maintain several metabolic functions, the liver consists of a few cell types that play distinct roles in hepatic homeostasis (Altin and Bygrave, 1988). Although parenchymal hepatocytes make up more than 85% of the liver, non-parenchymal cell types are known to be involved in liver regeneration (Michalopoulos, 2007). Indeed, several cholangiocyte-related diseases such as cystic fibrosis, Alagille syndrome, and primary sclerosing cholangitis exhibit severe liver dysfunction caused by abnormality in the bile ducts (Kobelska-Dubiel et al., 2014; Lindor et al., 2015; Turnpenny and Ellard, 2012), indicating the need for a novel approach for obtaining functional cholangiocytes with high purity. For this, Yu et al. (2013) demonstrated the direct generation of iHepSCs from mouse fibroblasts using *Hnf1β* and *Foxa3*. Although the previous study clearly characterized the bipotency of the iHepSCs, the conversion efficiency into iHepSCs was too low (less than 0.5%), with unusually extremely low differentiation potential into cholangiocytes (less than 2%). In the current study, we found that the combination of *Hnf1α* and *Foxa3* is sufficient for the robust generation of bipotential iHepSCs with 3.2- to 6.8-fold increased conversion efficiency compared with the previously defined combination (Figure 3). Throughout our mechanistic and functional studies, we observed that 1a3-iHepSCs are superior to 1b3-derived iHepSCs in their gene expression profile (Figures 4A, 4B, and 4D), conversion kinetics (Figures 3C and 3D), and both *in vitro* and *in vivo* differentiation potential into cholangiocytes (Figures 5 and 7), indicating that *Hnf1α* is a master factor for inducing hepatic stemness in somatic cells.

Previous *in vivo* studies might indirectly suggest a distinct role for each transcription factor (*Hnf1α*, *Hnf1β*, and *Foxa3*) in the generation of iHepSCs. *Foxa3* is a pioneer factor that belongs to the Foxa subfamily of winged helix/forkhead box transcription factors, which are known to guide many transcription factors in accessing their targets during liver development and regeneration (Kaestner et al., 1994; Lee et al., 2005; Wangensteen et al., 2015), suggesting its potential and essential role in iHepSC generation. However, *Hnf1β* is essential for the earliest step of hepatic bud formation, as its depletion leads the embryonic lethality (Coffinier et al., 2002; Lokmane et al., 2008), indicating that *Hnf1β* plays a critical role in early liver development. In contrast, *Hnf1α* is known to play a critical role in liver regeneration (Fausto, 2004; Leu et al., 2001; Nagy et al., 1994), despite its dispensable role in liver development (Pontoglio et al., 1996). Upon liver injury, HNF1A is known to directly bind to STAT3 and AP-1, resulting in the activation of several regeneration-associated hepatic genes (Leu

Figure 6. Notch-Mediated Secondary Conversion of 1a3-iHepSCs into Cholangiocyte Progenitor-like Cells

(A) Expression patterns of markers were evaluated in iHepSC lines from different passages by qPCR. All values were normalized to those of MEFs and are presented as mean ± SD from four biological replicates at each passage. Paired t test: *p < 0.05, **p < 0.01, ***p < 0.001.

(B) Immunofluorescence of 1a3-iHepSCs at different passages. Scale bar, 100 μm.

(C and D) Expression of hepatocyte-specific (C) and cholangiocyte-specific (D) markers in 1a3-iHepSCs was measured by qPCR. 1a3-iHepSCs were cultured in the absence or presence of 20 nM DAPT, a γ-secretase inhibitor of Notch signaling, during 10 serial passages from P1 to P10 (P10) and from P10 to 20 (P20). All values were normalized to those of MEFs and are presented as mean ± SD from three biological replicates. Paired t test: *p < 0.05, **p < 0.01; n.s., not significant.

(E) Immunofluorescence of iHepSCs cultured in the absence or presence of 20 nM DAPT. Scale bar, 100 μm.

(F) Graphical abstract describing two-step conversion strategy for generating iCPCs. Fibroblasts were converted primarily to bipotential hepatic stem cells by the ectopic expression of defined factors *Hnf1α* and *Foxa3*, then subjected to a secondary conversion process toward unipotent CPCs by spontaneous activation of Notch signaling.

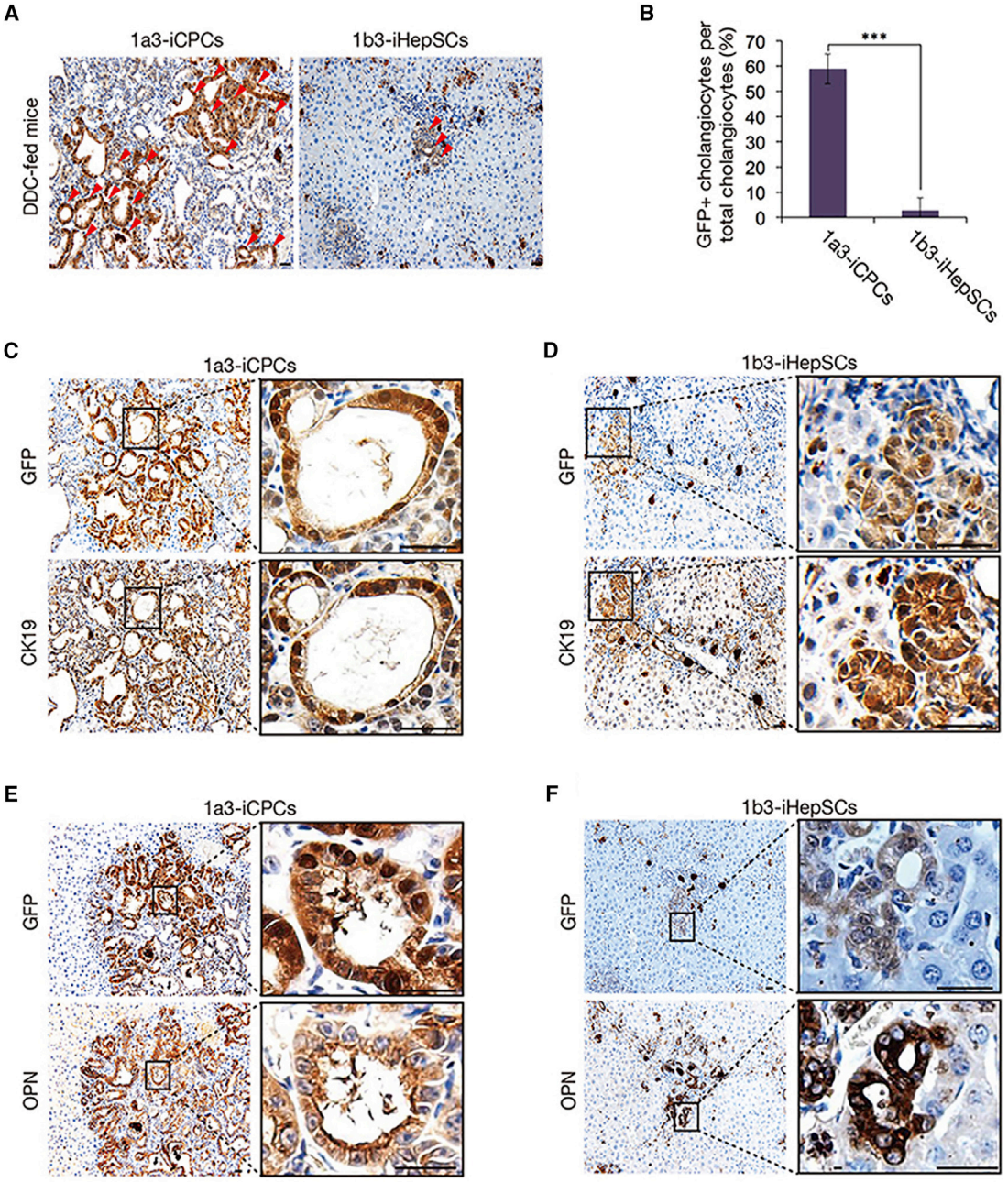

Figure 7. Robust Differentiation of 1a3-iCPCs into Mature Cholangiocytes

(A) Following transplantation, the engrafted GFP-labeled iCPCs and iHepSCs were differentiated into cholangiocytes (red arrowheads) in the bile ducts of livers of DDC-fed mice. Scale bars, 100 μm.

(B) Efficiency of differentiation into cholangiocytes was measured by counting the number of GFP^+ cholangiocytes per total number of cholangiocytes in the liver sections (1a3-iCPCs: 58.9% ± 5.9% versus 1b3-iHepSCs: 2.9% ± 5.0%). Data are presented as mean ± SD from three independent samples. Two-tailed Student's t test: ***$p < 0.001$.

(C–F) The GFP^+ cells in the bile ducts expressed mature cholangiocyte markers, CK19 (C and D) and OPN (E and F), as shown by immunohistochemistry. The images were obtained from serially sectioned slides. Scale bars, 100 μm.

et al., 2001), suggesting that *Hnf1α* plays a key role in liver regeneration. Importantly, *Hnf1α*, together with *Foxa3*, is activated specifically during oval cell proliferation; oval cells are the prototype adult liver progenitor cell population (Fausto, 2004; Nagy et al., 1994). Indeed, in the adult livers undergoing rapid regeneration process after 70%

partial hepatectomy (PHx), the expression of *Hnf1α* preceded that of *Hnf1β*; *Hnf1α* was immediately activated after PHx, while *Hnf1β* was slowly and progressively upregulated (Figure S7E). Considering that *Hnf1α* and *Foxa3* together lead the robust induction of hepatic stemness (Figure 3), 1a3-mediated direct conversion process toward an iHepSC state may share a similar pathway with the *in vivo* liver regeneration event that is orchestrated by both *Hnf1α* and *Foxa3*.

Furthermore, prolonged *in vitro* culture of 1a3-iHepSCs could induce the Notch signaling-mediated secondary conversion of 1a3-iHepSCs into unipotent iCPCs. Upon *in vitro* differentiation of 1a3-iCPCs into mature cholangiocytes, we observed bile duct proliferation (Figure S7F), a typical regenerative response to liver injury (Verdonk et al., 2016), suggesting that 1a3-iCPCs hold clinical potential for modeling various forms of liver diseases caused by cholangiocyte dysfunction. Further efforts in generating human iHepSCs/iCPCs and applying this technology for modeling genetic cholangiocyte-related diseases would essentially be required for successfully translating iHepSC/iCPC technology to the clinic.

EXPERIMENTAL PROCEDURES

Mice and Derivation of Fibroblasts

All mice used were bred and housed at the mouse facility of Konkuk University (KU) or at the Chinese Academy of Science (CAS). Animal handling was in accordance with both the KU and CAS animal protection guidelines. MEFs were derived on embryonic day 13.5 after removing the head and all internal organs, including the liver, from C57/B6 mouse strain embryos, and were cultured in DMEM (Hyclone) containing 10% fetal bovine serum and 5 mL of penicillin/streptomycin/glutamine (Invitrogen).

SUPPLEMENTAL INFORMATION

Supplemental Information includes Supplemental Experimental Procedures, seven figures, and two tables and can be found with this article online at https://doi.org/10.1016/j.stemcr.2018.03.002.

AUTHOR CONTRIBUTIONS

K.T.L., J.K., and S.I.H. performed the experiments and analyzed and interpreted the results. L.Z. and L.H. performed cell transplantation and analyzed the data. H.H., D.B., and I.L. analyzed the RNA sequencing data. K.-P.K. and H.R.S. analyzed and interpreted results. Y.-P.H. kindly provided the LEPCs. D.W.H. conceived and supervised the study and wrote the manuscript.

ACKNOWLEDGMENTS

This work was supported by National Research Foundation of Korea (NRF) grants funded by the Korean government (MSIP) (NRF-2016K1A3A1A61006005, NRF-2016R1A2B3011860, NRF-2016R1A5A2012284, and NRF-2017M3C7A1047640) and a grant from the Next-Generation BioGreen21 program (PJ011311), Rural Development Administration, Republic of Korea.

Received: October 28, 2017
Revised: March 4, 2018
Accepted: March 5, 2018
Published: March 29, 2018

REFERENCES

Altin, J.G., and Bygrave, F.L. (1988). Non-parenchymal cells as mediators of physiological responses in liver. Mol. Cell. Biochem. *83*, 3–14.

Alvaro, D., Mancino, M.G., Glaser, S., Gaudio, E., Marzioni, M., Francis, H., and Alpini, G. (2007). Proliferating cholangiocytes: a neuroendocrine compartment in the diseased liver. Gastroenterology *132*, 415–431.

Cahan, P., Li, H., Morris, S.A., Lummertz da Rocha, E., Daley, G.Q., and Collins, J.J. (2014). CellNet: network biology applied to stem cell engineering. Cell *158*, 903–915.

Coffinier, C., Gresh, L., Fiette, L., Tronche, F., Schütz, G., Babinet, C., Pontoglio, M., Yaniv, M., and Barra, J. (2002). Bile system morphogenesis defects and liver dysfunction upon targeted deletion of HNF1beta. Development *129*, 1829–1838.

Dhawan, A., Puppi, J., Hughes, R.D., and Mitry, R.R. (2010). Human hepatocyte transplantation: current experience and future challenges. Nat. Rev. Gastroenterol. Hepatol. *7*, 288–298.

Du, Y., Wang, J., Jia, J., Song, N., Xiang, C., Xu, J., Hou, Z., Su, X., Liu, B., Jiang, T., et al. (2014). Human hepatocytes with drug metabolic function induced from fibroblasts by lineage reprogramming. Cell Stem Cell *14*, 394–403.

Fausto, N. (2004). Liver regeneration and repair: hepatocytes, progenitor cells, and stem cells. Hepatology *39*, 1477–1487.

Forbes, S.J., Gupta, S., and Dhawan, A. (2015). Cell therapy for liver disease: from liver transplantation to cell factory. J. Hepatol. *62*, S157–S169.

Geisler, F., Nagl, F., Mazur, P.K., Lee, M., Zimber-Strobl, U., Strobl, L.J., Radtke, F., Schmid, R.M., and Siveke, J.T. (2008). Liver-specific inactivation of Notch2, but not Notch1, compromises intrahepatic bile duct development in mice. Hepatology *48*, 607–616.

Hay, D.C., Zhao, D., Fletcher, J., Hewitt, Z.A., McLean, D., Urruticoechea-Uriguen, A., Black, J.R., Elcombe, C., Ross, J.A., Wolf, R., and Cui, W. (2008). Efficient differentiation of hepatocytes from human embryonic stem cells exhibiting markers recapitulating liver development in vivo. Stem Cells *26*, 894–902.

He, J., Lu, H., Zou, Q., and Luo, L. (2014). Regeneration of liver after extreme hepatocyte loss occurs mainly via biliary transdifferentiation in zebrafish. Gastroenterology *146*, 789–800.e8.

Huang, P., He, Z., Ji, S., Sun, H., Xiang, D., Liu, C., Hu, Y., Wang, X., and Hui, L. (2011). Induction of functional hepatocyte-like cells from mouse fibroblasts by defined factors. Nature *475*, 386–389.

Huang, P., Zhang, L., Gao, Y., He, Z., Yao, D., Wu, Z., Cen, J., Chen, X., Liu, C., Hu, Y., et al. (2014). Direct reprogramming of human

fibroblasts to functional and expandable hepatocytes. Cell Stem Cell *14*, 370–384.

Kaestner, K.H., Hiemisch, H., Luckow, B., and Schutz, G. (1994). The HNF-3 gene family of transcription factors in mice: gene structure, cDNA sequence, and mRNA distribution. Genomics *20*, 377–385.

Kim, J., Kim, K.P., Lim, K.T., Lee, S.C., Yoon, J., Song, G., Hwang, S.I., Scholer, H.R., Cantz, T., and Han, D.W. (2015). Generation of integration-free induced hepatocyte-like cells from mouse fibroblasts. Sci. Rep. *5*, 15706.

Kobelska-Dubiel, N., Klincewicz, B., and Cichy, W. (2014). Liver disease in cystic fibrosis. Prz. Gastroenterol. *9*, 136–141.

Lee, C.S., Friedman, J.R., Fulmer, J.T., and Kaestner, K.H. (2005). The initiation of liver development is dependent on Foxa transcription factors. Nature *435*, 944–947.

Leu, J.I., Crissey, M.A., Leu, J.P., Ciliberto, G., and Taub, R. (2001). Interleukin-6-induced STAT3 and AP-1 amplify hepatocyte nuclear factor 1-mediated transactivation of hepatic genes, an adaptive response to liver injury. Mol. Cell. Biol. *21*, 414–424.

Li, F., Liu, P., Liu, C., Xiang, D., Deng, L., Li, W., Wangensteen, K., Song, J., Ma, Y., Hui, L., et al. (2010). Hepatoblast-like progenitor cells derived from embryonic stem cells can repopulate livers of mice. Gastroenterology *139*, 2158–2169.e8.

Li, W.L., Su, J., Yao, Y.C., Tao, X.R., Yan, Y.B., Yu, H.Y., Wang, X.M., Li, J.X., Yang, Y.J., Lau, J.T., et al. (2006). Isolation and characterization of bipotent liver progenitor cells from adult mouse. Stem Cells *24*, 322–332.

Lim, K.T., Lee, S.C., Gao, Y., Kim, K.P., Song, G., An, S.Y., Adachi, K., Jang, Y.J., Kim, J., Oh, K.J., et al. (2016). Small molecules facilitate single factor-mediated hepatic reprogramming. Cell Rep. *15*, 814–829.

Lindor, K.D., Kowdley, K.V., and Harrison, M.E.; American College of Gastroenterology (2015). ACG clinical guideline: primary sclerosing cholangitis. Am. J. Gastroenterol. *110*, 646–659, quiz 660.

Lokmane, L., Haumaitre, C., Garcia-Villalba, P., Anselme, I., Schneider-Maunoury, S., and Cereghini, S. (2008). Crucial role of vHNF1 in vertebrate hepatic specification. Development *135*, 2777–2786.

Michalopoulos, G.K. (2007). Liver regeneration. J. Cell. Physiol. *213*, 286–300.

Nagy, P., Bisgaard, H.C., and Thorgeirsson, S.S. (1994). Expression of hepatic transcription factors during liver development and oval cell differentiation. J. Cell Biol. *126*, 223–233.

Ogawa, M., Ogawa, S., Bear, C.E., Ahmadi, S., Chin, S., Li, B., Grompe, M., Keller, G., Kamath, B.M., and Ghanekar, A. (2015). Directed differentiation of cholangiocytes from human pluripotent stem cells. Nat. Biotechnol. *33*, 853–861.

Pontoglio, M., Barra, J., Hadchouel, M., Doyen, A., Kress, C., Bach, J.P., Babinet, C., and Yaniv, M. (1996). Hepatocyte nuclear factor 1 inactivation results in hepatic dysfunction, phenylketonuria, and renal Fanconi syndrome. Cell *84*, 575–585.

Preisegger, K.H., Factor, V.M., Fuchsbichler, A., Stumptner, C., Denk, H., and Thorgeirsson, S.S. (1999). Atypical ductular proliferation and its inhibition by transforming growth factor beta1 in the 3,5-diethoxycarbonyl-1,4-dihydrocollidine mouse model for chronic alcoholic liver disease. Lab. Invest. *79*, 103–109.

Sampaziotis, F., de Brito, M.C., Madrigal, P., Bertero, A., Saeb-Parsy, K., Soares, F.A., Schrumpf, E., Melum, E., Karlsen, T.H., Bradley, J.A., et al. (2015). Cholangiocytes derived from human induced pluripotent stem cells for disease modeling and drug validation. Nat. Biotechnol. *33*, 845–852.

Sekiya, S., and Suzuki, A. (2011). Direct conversion of mouse fibroblasts to hepatocyte-like cells by defined factors. Nature *475*, 390–393.

Si-Tayeb, K., Noto, F.K., Nagaoka, M., Li, J., Battle, M.A., Duris, C., North, P.E., Dalton, S., and Duncan, S.A. (2010). Highly efficient generation of human hepatocyte-like cells from induced pluripotent stem cells. Hepatology *51*, 297–305.

Tang, C., Lee, A.S., Volkmer, J.P., Sahoo, D., Nag, D., Mosley, A.R., Inlay, M.A., Ardehali, R., Chavez, S.L., Pera, R.R., et al. (2011). An antibody against SSEA-5 glycan on human pluripotent stem cells enables removal of teratoma-forming cells. Nat. Biotechnol. *29*, 829–834.

Tanimizu, N., Miyajima, A., and Mostov, K.E. (2007). Liver progenitor cells develop cholangiocyte-type epithelial polarity in three-dimensional culture. Mol. Biol. Cell *18*, 1472–1479.

Turnpenny, P.D., and Ellard, S. (2012). Alagille syndrome: pathogenesis, diagnosis and management. Eur. J. Hum. Genet. *20*, 251–257.

Verdonk, R.C., Lozano, M.F., van den Berg, A.P., and Gouw, A.S. (2016). Bile ductal injury and ductular reaction are frequent phenomena with different significance in autoimmune hepatitis. Liver Int. *36*, 1362–1369.

Walter, T.J., Vanderpool, C., Cast, A.E., and Huppert, S.S. (2014). Intrahepatic bile duct regeneration in mice does not require Hnf6 or Notch signaling through Rbpj. Am. J. Pathol. *184*, 1479–1488.

Wangensteen, K.J., Zhang, S., Greenbaum, L.E., and Kaestner, K.H. (2015). A genetic screen reveals Foxa3 and TNFR1 as key regulators of liver repopulation. Genes Dev. *29*, 904–909.

Yu, B., He, Z.Y., You, P., Han, Q.W., Xiang, D., Chen, F., Wang, M.J., Liu, C.C., Lin, X.W., Borjigin, U., et al. (2013). Reprogramming fibroblasts into bipotential hepatic stem cells by defined factors. Cell Stem Cell *13*, 328–340.

Zhang, W., Li, W., Liu, B., Wang, P., Li, W., and Zhang, H. (2012). Efficient generation of functional hepatocyte-like cells from human fetal hepatic progenitor cells in vitro. J. Cell. Physiol. *227*, 2051–2058.

Stem Cell Reports, Volume *10*

Supplemental Information

Direct Conversion of Mouse Fibroblasts into Cholangiocyte Progenitor Cells

Kyung Tae Lim, Jonghun Kim, Seon In Hwang, Ludi Zhang, Heonjong Han, Dasom Bae, Kee-Pyo Kim, Yi-Ping Hu, Hans R. Schöler, Insuk Lee, Lijian Hui, and Dong Wook Han

Supplemental Information

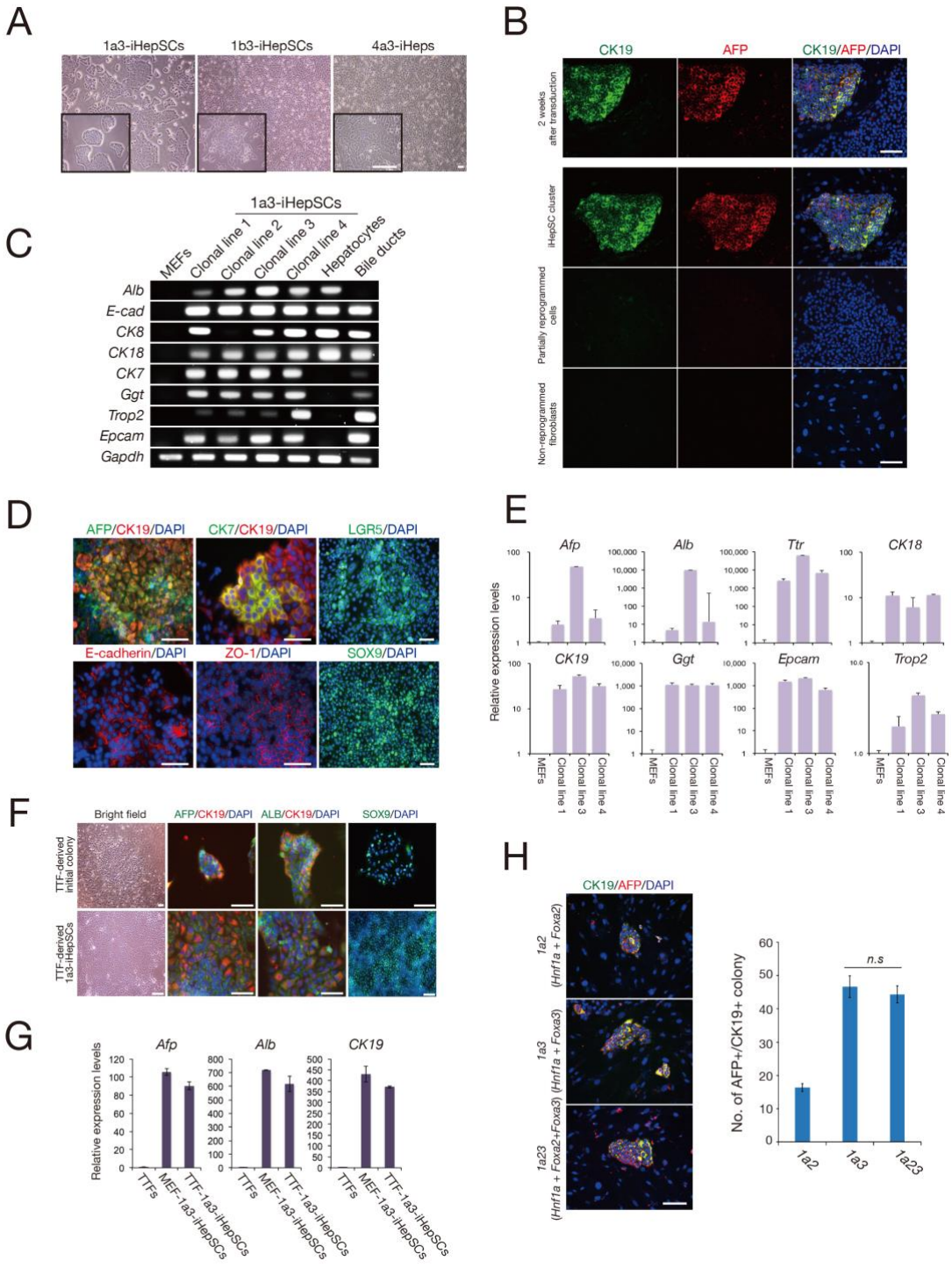

Figure S1. Characterization of 1a3-iHepSCs. Related to Figure 1.

(A**)** Morphology of established 1a3-iHepSCs, 1b3-iHepSCs, and 4a3-iHeps, as assessed by bright-field microscopy. Scale bars, 100 μm. (B) Morphology and marker expression of reprogrammed iHepSCs, partially reprogrammed cells, and non-reprogrammed fibroblasts. Scale bars, 100 μm. (C**)** Expression patterns of hepatocyte-, cholangiocyte-, and HepSC-specific markers were analyzed by RT-PCR. (D**)** Immunofluorescence of established 1a3-iHepSCs using antibodies directed against AFP, CK19, CK7, E-cadherin, ZO-1, LGR5, and/or SOX9. The nuclei were stained with DAPI. Scale bars, 100 μm. (E**)** Expression levels of hepatocyte-, cholangiocyte-, and HepSC-specific markers in three independent clonal 1a3-iHepSC lines were measured by qPCR. The expression levels were normalized to those of MEFs and are represented as mean ± SD of triplicate values. (F**)** Generation of adult mouse tail-tip fibroblast (TTF)-derived iHepSCs by 1a3. The TTF-derived 1a3-iHepSCs at passage 12 were stained using antibodies directed against AFP, ALB, CK19, and/or SOX9. The nuclei were stained with DAPI. Scale bars represent 100 μm. (G**)** Expression levels of hepatocyte-, cholangiocyte-, and HepSC-specific markers in TTF-derived 1a3-iHepSCs as measured by qPCR. The expression levels were normalized to those of MEFs and are represented as mean ± SD of triplicate values. (H) Conversion efficiency into iHepSCs after 2 weeks of transducing distinct factor combinations (1a2, 1a3, and 1a23). Data are represented as mean ± SD from three independent experiments. Two-tailed Student *t*-test: *n.s.*, not significant.

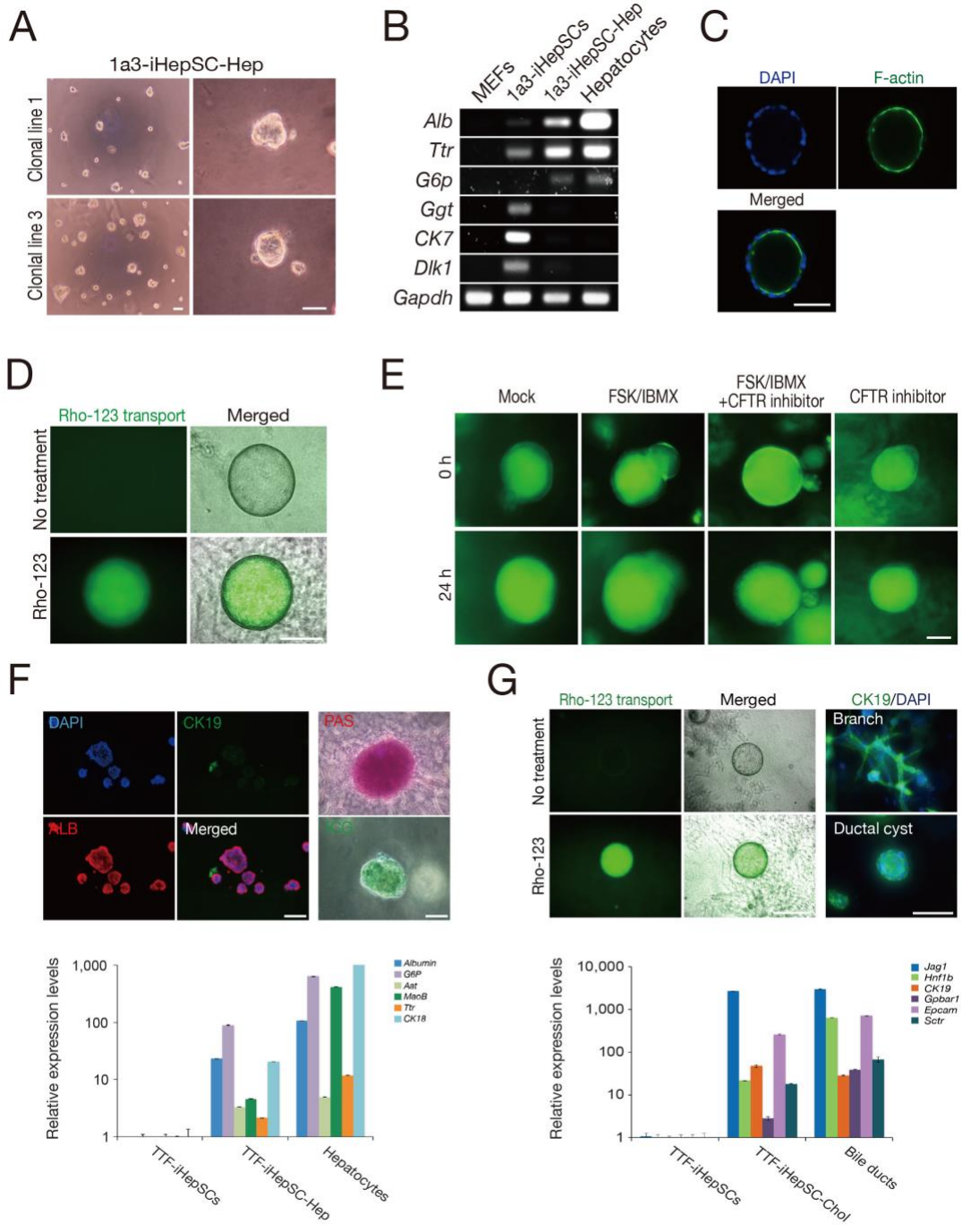
A
1a3-iHepSC-Hep
Clonal line 1
Clonal line 3
B
MEFs
1a3-iHepSCs
1a3-iHepSC-Hep
Hepatocytes
Alb
Ttr
G6p
Ggt
CK7
Dlk1
Gapdh
C
DAPI
F-actin
Merged
D
Rho-123 transport
Merged
No treatment
Rho-123
E
Mock
FSK/IBMX
FSK/IBMX +CFTR inhibitor
CFTR inhibitor
0 h
24 h
F
DAPI
CK19
PAS
ALB
Merged
PAS
Relative expression levels
1,000
100
10
1
Albumin
G6P
Aat
MaoB
Ttr
CK18
TTF-iHepSCs
TTF-iHepSC-Hep
Hepatocytes
G
Rho-123 transport
Merged
CK19/DAPI
No treatment
Rho-123
Branch
Ductal cyst
Relative expression levels
10,000
1,000
100
10
1
Jag1
Hnf1b
CK19
Gpbar1
Epcam
Sctr
TTF-iHepSCs
TTF-iHepSC-Chol
Bile ducts

Figure S2. Differentiation potential of 1a3-iHepSCs. Related to Figure 2.

(A**)** Morphology of 1a3-iHepSC–derived hepatocytes was assessed by bright-field microscopy. (B**)** Expression patterns of hepatocyte- and cholangiocyte-specific markers were evaluated by RT-PCR. MEFs and primary hepatocytes were used as negative and positive controls, respectively. (C**)** Immunostaining images of F-actin in 1a3-iHepSC–derived ductal cysts. Nuclei were stained with DAPI. (D**)** Transport of Rho123 into the central lumen of a ductal cyst. (E**)** Fluorescence microscopy images of 1a3-iHepSC–derived ductal cysts before and after FSK and IBMX stimulation in the absence or presence of the CFTR inhibitor. Scale bars, 100 μm. (F, G) Differentiation of TTF-iHepSCs into hepatocytes (F) and cholangiocytes (G).

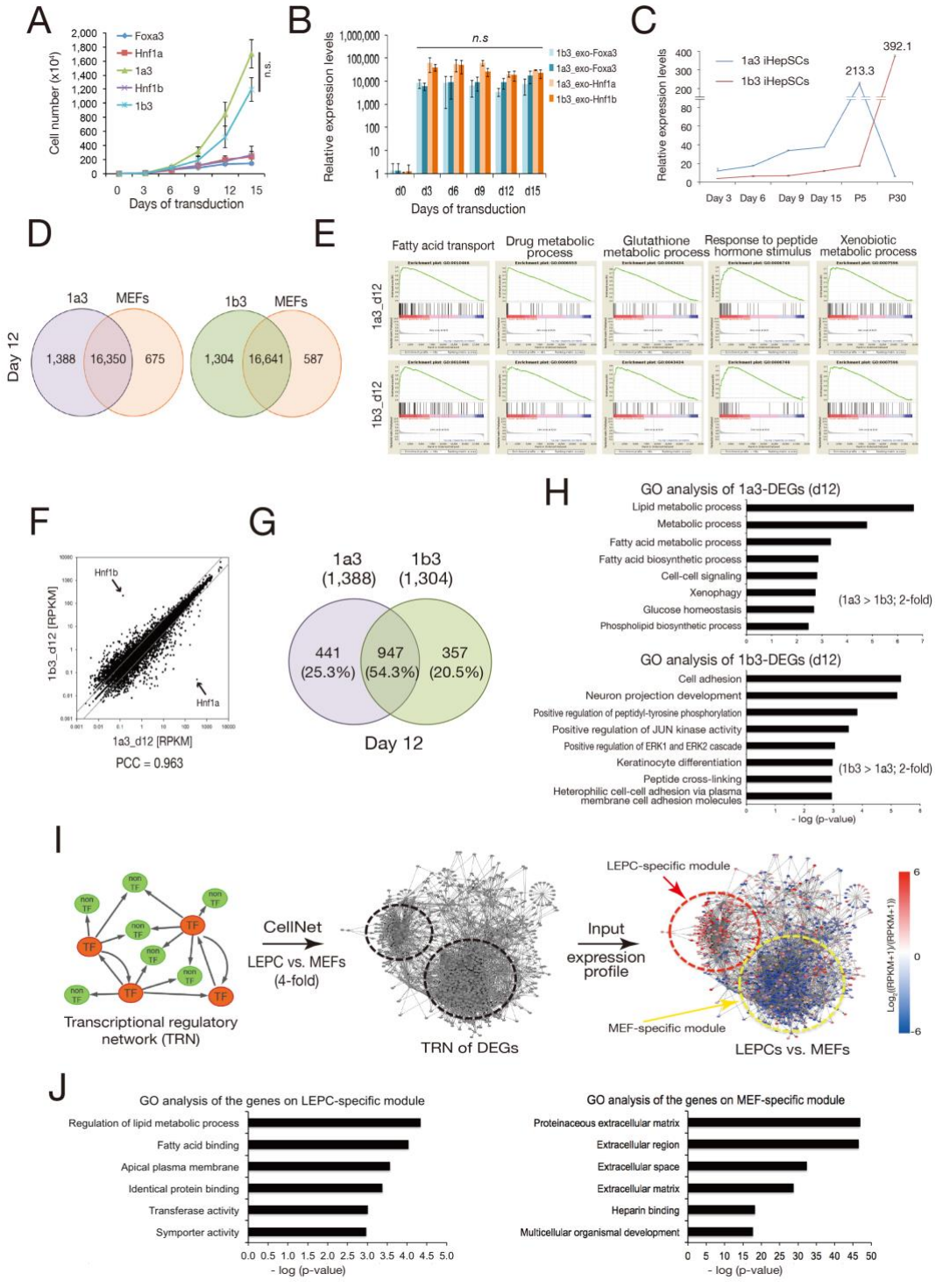
A
Cell number (x10⁴)
Foxa3
Hnf1a
1a3
Hnf1b
1b3
n.s.
Days of transduction
B
Relative expression levels
n.s
1b3_exo-Foxa3
1a3_exo-Foxa3
1a3_exo-Hnf1a
1b3_exo-Hnf1b
d0 d3 d6 d9 d12 d15
Days of transduction
C
Relative expression levels
1a3 iHepSCs
1b3 iHepSCs
213.3
392.1
Day 3 Day 6 Day 9 Day 15 P5 P30
D
Day 12
1a3 MEFs
1,388 16,350 675
1b3 MEFs
1,304 16,641 587
E
Fatty acid transport
Drug metabolic process
Glutathione metabolic process
Response to peptide hormone stimulus
Xenobiotic metabolic process
1a3_d12
1b3_d12
F
Hnf1b
Hnf1a
1b3_d12 [RPKM]
1a3_d12 [RPKM]
PCC = 0.963
G
1a3 (1,388)
1b3 (1,304)
441 (25.3%)
947 (54.3%)
357 (20.5%)
Day 12
H
GO analysis of 1a3-DEGs (d12)
Lipid metabolic process
Metabolic process
Fatty acid metabolic process
Fatty acid biosynthetic process
Cell-cell signaling
Xenophagy
Glucose homeostasis
Phospholipid biosynthetic process
(1a3 > 1b3; 2-fold)
GO analysis of 1b3-DEGs (d12)
Cell adhesion
Neuron projection development
Positive regulation of peptidyl-tyrosine phosphorylation
Positive regulation of JUN kinase activity
Positive regulation of ERK1 and ERK2 cascade
Keratinocyte differentiation
Peptide cross-linking
Heterophilic cell-cell adhesion via plasma membrane cell adhesion molecules
(1b3 > 1a3; 2-fold)
- log (p-value)
I
non TF
TF
Transcriptional regulatory network (TRN)
CellNet
LEPC vs. MEFs (4-fold)
TRN of DEGs
Input expression profile
LEPC-specific module
MEF-specific module
LEPCs vs. MEFs
Log2((RPKM+1)/(RPKM+1))
J
GO analysis of the genes on LEPC-specific module
Regulation of lipid metabolic process
Fatty acid binding
Apical plasma membrane
Identical protein binding
Transferase activity
Symporter activity
- log (p-value)
GO analysis of the genes on MEF-specific module
Proteinaceous extracellular matrix
Extracellular region
Extracellular space
Extracellular matrix
Heparin binding
Multicellular organismal development
- log (p-value)

Figure S3. Faster induction of hepatic stemness by *Foxa3* and *Hnf1α*. Related to Figure 3.

(A, B**)** Proliferation rate of the cells (A) and expression levels of transgenes (B) were monitored in a time-course manner, on days 3, 6, 9, 12, and 15 after transduction of MEFs with the reprogramming factors. Data are represented as mean ± SD of triplicate values from three independent samples. Two-way ANOVA, One-way ANOVA, respectively: **P*<0.05; *n.s.*, not significant. (C) Transcriptional kinetic analysis of CPM (carboxypeptidase M) during iHepSC generation. The levels were normalized to those of MEFs and are represented as mean ± SD of triplicate values. (D**)** Venn diagram representing the number of differentially expressed genes upon induction of each reprogramming cocktail, 1a3 (*left*) or 1b3 (*right*), after 12 days of transduction, respectively. (E**)** Gene set enrichment analysis (GSEA) of 1a3- or 1b3-transduced cells on day 12 post-infection, which showed remarkable enrichment of diverse biological processes in Gene Ontology (GO) involved in liver functions. A peak shift to the left side indicates that genes involved in the processes are upregulated in 1a3- or 1b3-transduced cells, respectively. (F**)** A scatter plot of the expression patterns of genes in 1a3-transduced cells compared with those in 1b3-transduced cells on day 12 post-infection. Pearson correlation coefficient close to +1 indicates that there is a strong positive correlation between the two samples. (G**)** Venn diagram describing the number of up-regulated genes in 1a3- and 1b3-transduced cells after 12 days of transduction (fold change >2; *P*<0.05). (H**)** GO enrichment analyses of differentially expressed genes (DEGs) by 2 fold between 1a3- and 1b3-transduced cells on day 12 post-infection. (I**)** A transcriptional regulatory network (TRN) extracted from CellNet using differentially expressed genes between liver epithelial progenitor cells (LEPCs) and MEFs by 4 fold. The TRN consists of distinct modules that are specific for MEF- and LEPC-specific modules, *yellow* and *red* dotted circles, respectively. (J**)** GO analyses of MEF- and LEPC-specific modules. Biological process terms were analyzed based on the gene enrichment score: –log (*P*-value).

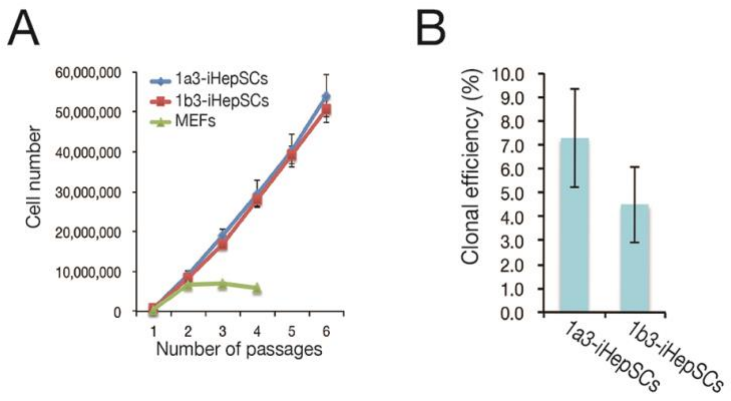
A
B
1a3-iHepSCs
1b3-iHepSCs
MEFs
Cell number
60,000,000
50,000,000
40,000,000
30,000,000
20,000,000
10,000,000
0
1
2
3
4
5
6
Number of passages
Clonal efficiency (%)
10.0
9.0
8.0
7.0
6.0
5.0
4.0
3.0
2.0
1.0
0.0
1a3-iHepSCs
1b3-iHepSCs

Figure S4. Characterization of 1a3- and 1b3-iHepSCs. Related to Figure 4.

(A**)** Proliferation rate was monitored as the cells underwent a series of passages. Data are represented as mean ± SD of three biological samples. Two-tailed Student *t*-test: **P* < 0.05. (B**)** Clonal efficiency (%) was measured after 7 days of sorting single cells into 96-well dishes by flow cytometry. Data are represented as mean ± SD of three biological replicates. Two-tailed Student *t*-test: **P*<0.05.

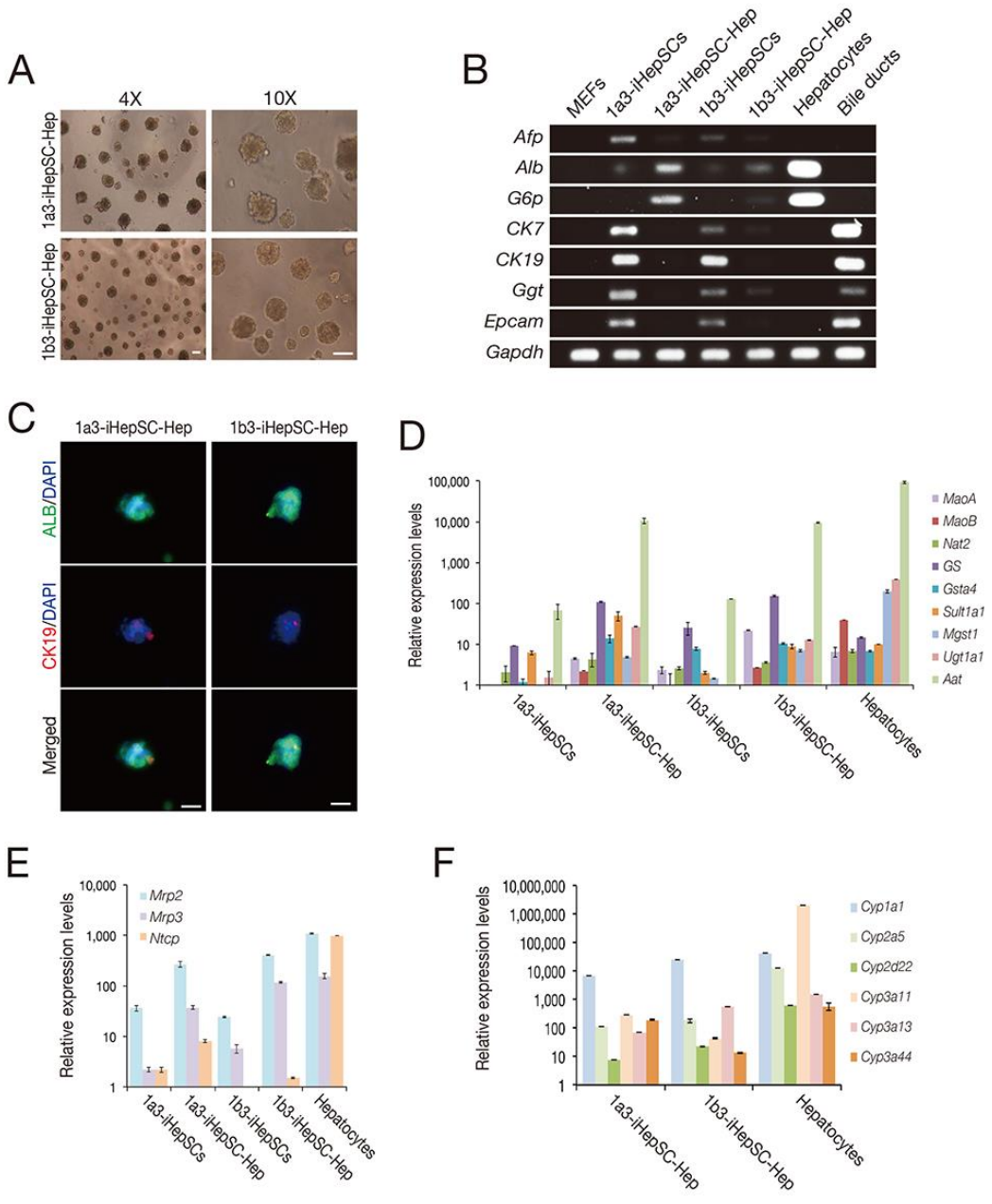
A
4X
10X
1a3-iHepSC-Hep
1b3-iHepSC-Hep
B
MEFs
1a3-iHepSCs
1a3-iHepSC-Hep
1b3-iHepSCs
1b3-iHepSC-Hep
Hepatocytes
Bile ducts
Afp
Alb
G6p
CK7
CK19
Ggt
Epcam
Gapdh
C
1a3-iHepSC-Hep
1b3-iHepSC-Hep
ALB/DAPI
CK19/DAPI
Merged
D
Relative expression levels
100,000
10,000
1,000
100
10
1
MaoA
MaoB
Nat2
GS
Gsta4
Sult1a1
Mgst1
Ugt1a1
Aat
1a3-iHepSCs
1a3-iHepSC-Hep
1b3-iHepSCs
1b3-iHepSC-Hep
Hepatocytes
E
Relative expression levels
10,000
1,000
100
10
1
Mrp2
Mrp3
Ntcp
1a3-iHepSCs
1a3-iHepSC-Hep
1b3-iHepSCs
1b3-iHepSC-Hep
Hepatocytes
F
Relative expression levels
10,000,000
1,000,000
100,000
10,000
1,000
100
10
1
Cyp1a1
Cyp2a5
Cyp2d22
Cyp3a11
Cyp3a13
Cyp3a44
1a3-iHepSC-Hep
1b3-iHepSC-Hep
Hepatocytes

Figure S5. Comparison of hepatic differentiation potential between 1a3- and 1b3-iHepSCs. Related to Figure 5.

(A**)** Morphology of 1a3-iHepSC– and 1b3-iHepSC–derived hepatocytes after 7 days of hepatic differentiation. Scale bars, 100 μm. (B**)** Expression patterns of hepatocyte- and cholangiocyte-specific markers were evaluated by RT-PCR. MEFs, primary hepatocytes, and bile duct tissues were used as negative and positive controls, respectively. Data are represented as mean ± SD of triplicate values. (C**)** Immunofluorescence of 1a3-iHepSC–derived hepatocytes after 7 days of iHepSC differentiation. Antibodies directed against ALB and CK19 were used. The nuclei were stained with DAPI. Scale bars, 100 μm. (D**)** Expression values of genes related to liver-specific enzymes were analyzed by qPCR. All the values were normalized to those of MEFs. MEFs and primary hepatocytes were used as negative and positive controls, respectively. Data are represented as mean ± SD of triplicate values. (E**)** Expression of drug transporter–related genes was measured in iHepSC-differentiated hepatocytes from three independent 1a3- and 1b3-iHepSC lines by qPCR. All the values were normalized to those of MEFs and are represented as mean ± SD of triplicate values. (F**)** Expression levels of Cyp450 enzymes in response to Cyp inducers (3-methylcholanthrene, rifampicin, and dexamethasone) were evaluated by qPCR after 7 days of hepatic differentiation. All values were normalized to those of iHepSCs before differentiation, and are represented as mean ± SD of triplicate values.

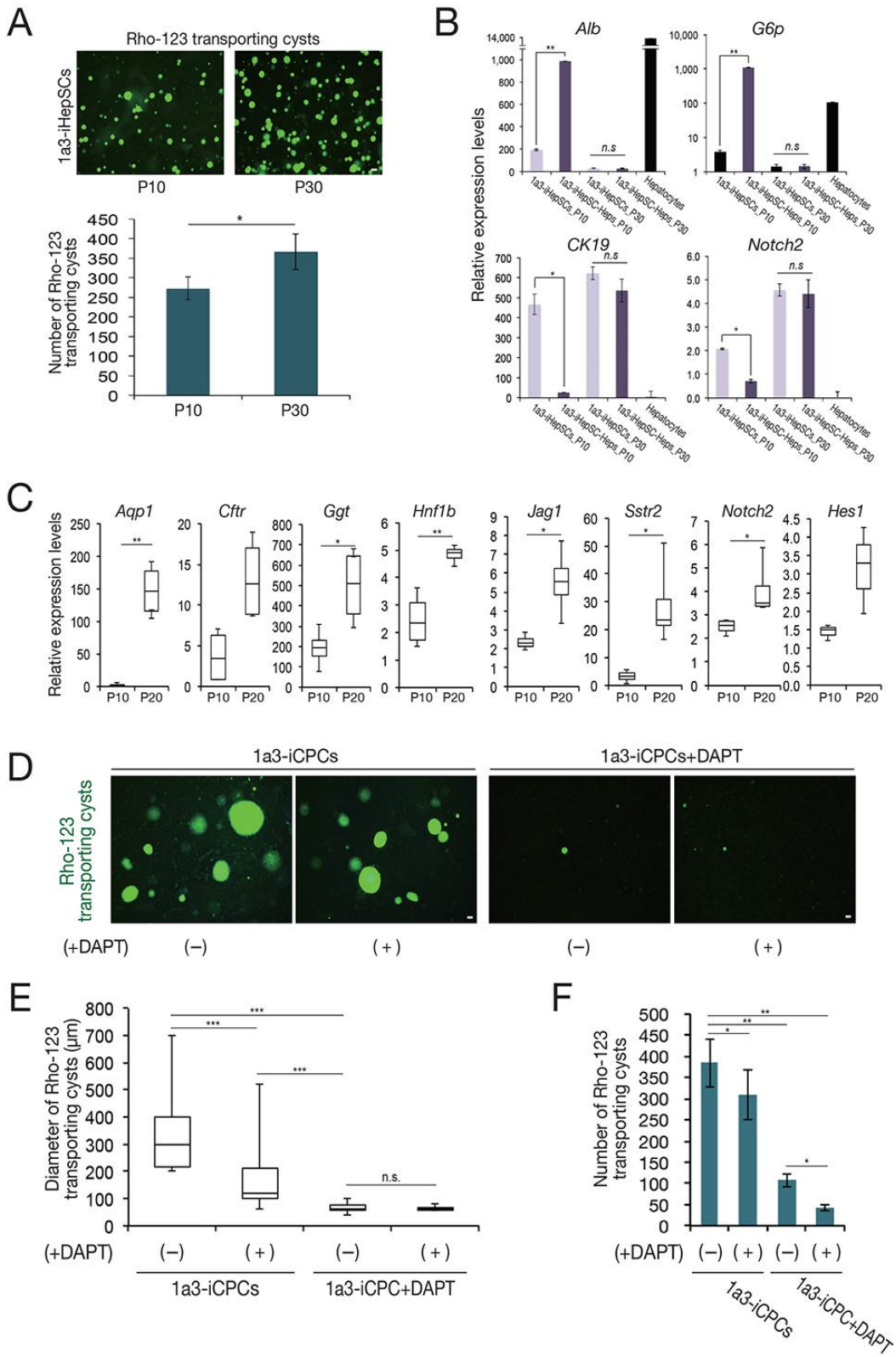
A
Rho-123 transporting cysts
1a3-iHepSCs
P10
P30
Number of Rho-123 transporting cysts
B
Alb
G6p
CK19
Notch2
Relative expression levels
1a3-iHepSCs_P10
1a3-iHepSC-Heps_P10
1a3-iHepSCs_P30
1a3-iHepSC-Heps_P30
Hepatocytes
n.s
C
Aqp1
Cftr
Ggt
Hnf1b
Jag1
Sstr2
Notch2
Hes1
Relative expression levels
P10
P20
D
1a3-iCPCs
1a3-iCPCs+DAPT
Rho-123 transporting cysts
(+DAPT)
(–)
(+)
E
Diameter of Rho-123 transporting cysts (μm)
n.s.
(+DAPT)
(–)
(+)
1a3-iCPCs
1a3-iCPC+DAPT
F
Number of Rho-123 transporting cysts
(+DAPT)
(–)
(+)
1a3-iCPCs
1a3-iCPC+DAPT

Figure S6. Notch-mediated secondary conversion of 1a3-iHepSCs into cholangiocyte progenitor–like cells. Related to Figure 6.

(A**)** *In vitro* differentiation of 1a3-iHepSCs at early and late passages (P10 and P30), respectively. The number of Rho123-transporting cysts was measured on 7 days of differentiation. Data are represented as mean ± SD of triplicate values from five biological replicates. Paired *t*-test: **P*<0.05. (B) Expression levels of the markers of mature hepatocytes (*Alb*, *G6p*) and cholangiocytes (*CK19*, *Notch2*) in 1a3-iHepSCs (P10 and 30) were monitored by qPCR upon 7 days of hepatic differentiation. All the values were normalized to those of MEFs. Data are represented as mean ± SD of triplicate values from three biological replicates. Paired *t*-test: **P*<0.05; *n.s.*, not significant. (C**)** A box-and-whisker plot describing the expression levels of mature cholangiocyte-related genes measured by qPCR. Four biological replicates of 1a3-iHepSC lines on passage 10 (P10) were spontaneously differentiated into iCPCs during 10 passages (P20). All the values were normalized to those of MEFs. Paired *t*-test: **P*<0.05; ***P*<0.01; ****P*<0.001. (D-F**)** Transport of Rho123 into the central lumen of ductal cysts (D). 1a3-iCPCs pre-incubated in the absence or presence of 20 nM of DAPT with more than five serial passages were treated with or without DAPT during cholangiocyte differentiation *in vitro*. The diameter (E) and the number (F) of Rho123-transporting cysts were measured upon 7 days of differentiation. The diameter of the cysts is displayed in a box-and-whisker plot (E) and the number of cysts is represented as mean ± SD (F) from three biological replicates. Paired *t*-test: **P*<0.05; ***P*<0.01; ****P*<0.001; *n.s.*, not significant.

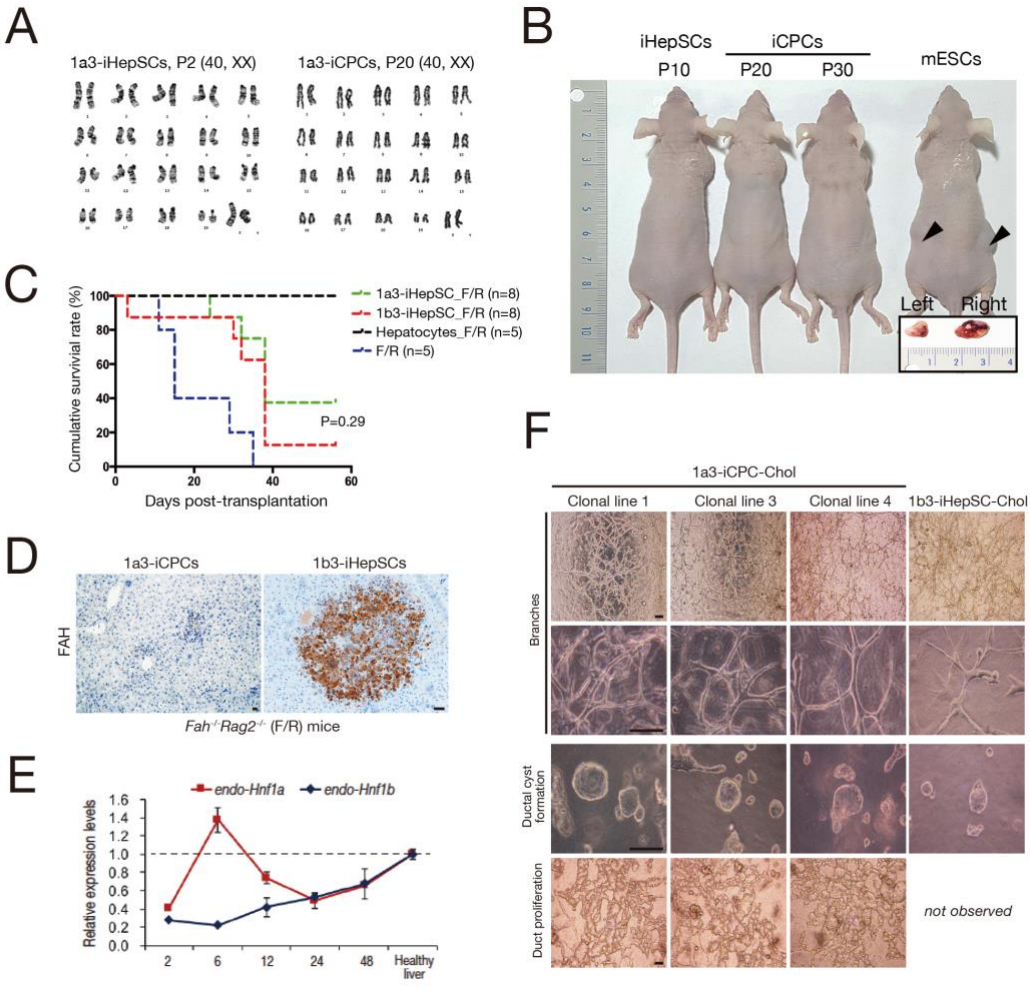
A
1a3-iHepSCs, P2 (40, XX)
1a3-iCPCs, P20 (40, XX)
B
iHepSCs
iCPCs
P10
P20
P30
mESCs
Left
Right
C
Cumulative survivial rate (%)
1a3-iHepSC_F/R (n=8)
1b3-iHepSC_F/R (n=8)
Hepatocytes_F/R (n=5)
F/R (n=5)
P=0.29
Days post-transplantation
D
1a3-iCPCs
1b3-iHepSCs
FAH
Fah-/-Rag2-/- (F/R) mice
E
endo-Hnf1a
endo-Hnf1b
Relative expression levels
Healthy liver
F
1a3-iCPC-Chol
Clonal line 1
Clonal line 3
Clonal line 4
1b3-iHepSC-Chol
Branches
Ductal cyst formation
Duct proliferation
not observed

Figure S7. Robust differentiation of iCPCs into mature cholangiocytes. Related to Figure 7.

(A) Karyotype analysis of iHepSCs and iCPCs. Both iHepSCs (passage 2) and iCPCs (passage 20) exhibited normal karyotypes. (B) Teratoma assay using both iHepSCs and iCPCs. 1 x 10^6 of iHepSCs (passage 10) or iCPCs (passages 20 and 30) were injected into the left and right sides of NOD/SCID mice subcutaneously. Mouse embryonic stem cells were also injected as a positive control. Arrow heads depict teratomas observed after 8 weeks of transplantation. (C) Cumulative survival blot of *Fah*$^{-/-}$/*Rag*$^{-/-}$ (F/R)- deficient mice after transplantation of iHepSCs. 1 × 10^6 of 1a3- and 1b3-iHepSCs were transplanted into *Fah*$^{-/-}$/*Rag*$^{-/-}$ (F/R)- deficient mice. **(**D**)** Repopulation of FAH-positive cells was analyzed by immunostaining using antibody directed against FAH at 8 weeks after transplantation of both iCPCs and iHepSCs. Scale bars, 100 μm. (E**)** Expression patterns of endogenous *Hnf1α* and *Hnf1β* upon 70% partial hepatectomy (PHx). The liver tissues were collected at 2, 6, 12, 24, and 48 h after PHx. All the values are normalized to the level of healthy liver. (F**)** Morphology of cholangiocytes that had differentiated from iCPCs and iHepSCs *in vitro*. Scale bars, 100 μm.

Table S1. Primers for analyzing the expression of marker genes. Related to Experimental procedures.

Gene Name	**Genebank Number**	**Primer sequences**
Aat	NM_009243	5’-CCTGCTAAACAGGCGCAGAA-3’ 5’-TCGATGGTCAGCACAGCCTTA-3’
Afp	NM_007423	5’-CGTGATGCTTTGGGCGTTTA-3’ 5’-GCCAAAAGGCTCACACCAAAG-3’
Alb	NM_009654	5’-AAACCTTGTCACTAGATGCAAAGACG-3’ 5’-GGGTAGCCTGAGAAGGTTGTGG-3’
Hnf1a	NM_009327	5’-CCTGCTGCCATCCAACCATA-3’ 5’-CCACGGTTACTGGGAAGAGGA-3’
Hnf4a	NM_008261	5’-GCCAACGATCACCAAGCAAG-3’ 5’-TGAGGGTATGAGCCAGCAGAA-3’
E-cadherin	NM_009864	5’-TTCAAGAAGCTGGCGGACAT-3’ 5’-CATCTCCCATGGTGCCACAC-3’
Ttr	NM_013697	5’-CCCTGCTCAGCCCATACTCCTA-3’ 5’-TGCTTTGGCAAGATCCTGGT-3’
CK18	NM_010664	5’-GATCGTGGATGGCAGAGTGG-3’ 5’-TTCCCTCCTTCTCTGCCTCAGT-3’
G6p	NM_008061	5’-CGGATCCTGGGACAGACACA-3’ 5’-CTTTGCATGGCGGTTGACTT-3’
CK19	NM_008471	5’-CCCCAAGGCCATCTGAGCTA-3’ 5’-GAGTAAACTTTTATCACCCCAGTCAGG-3’
CK7	NM_033073	5’-CCTCAGGGCCTATTCCATCAA-3’ 5’-GTCTCTCCAAGCCCACAGCTT-3’
Ggt	NM_008116	5’-CAGCTGCCTCAGACTCCAGAA-3’ 5’-TTCCCATTCTCGTCCCTTGG-3’
Trop2	NM_020047	5’-GAGATGAGAAGCGAACCTAGCTTGTAG-3’ 5’-AACTTGTTTGTGGAGAGAGAAGGAAGA-3’
Epcam	NM_008532	5’-GGTGGTGTCATTAGCAGTCATCG-3’ 5’-TGTGGATCTCACCCATCTCCTT-3’
Dlk1	NM_010052	5’-GGATTCTGCGAGGCTGACAA-3’ 5’-GCAGATGCACTGCCATGGTT-3’
Notch2	NM_010928	5’-TTTGTGTCCCGCCCTTGTC-3’ 5’-AGGGCATTTGCAGGAGAACTG-3’
Cftr	NM_021050	5’-CTGCTTGATGAGCCCAGTGC-3’ 5’-TGAAGGGAGTCGTACTGCCAGA-3’
Aqp1	NM_00747	5’-CGGTCATTTGGCTCTGCTGT-3’ 5’-CACTGGTCCACACCTTCATGC-3’
Hnf1b	NM_009330	5’-GTGTCCACTGCAAGCCTGG-3’ 5’-CCCAGAGACTGATGGTGTGGA-3’
Jag1	NM_013822	5’-ACCTGCGTGGTCAATGGAGA-3’ 5’-CACATTCGCACCGATACCAGTT-3’
Sstr2	NM_009217	5’-TGCTAGAGAACACAGGGAAGCGA-3’ 5’-TGTCGTAGTATGGCTCGGTCTGG-3’
Hes1	NM_008235	5’-GTGAAGCACCTCCGGAACCT-3’ 5’-CTCGTTCATGCACTCGCTGA-3’
Mdr1	NM_011075	5’-CGAAGCAACATCAGCTCTGGA-3’ 5’-CTTTGCTCCAGCCTGCACAC-3’
Gpbar1	NM_174985	5’-GTGGCCACATTGCTCCTGTC-3’ 5’-TGGCTCTTCCTCGAAGCACTC-3’
Sctr	NM_001012322	5’-CCATGGAGGTCCAGCTGTTCT-3’ 5’-CGTTGCTGAAGGAGTTGCTGA-3’
Slc4a2	NM_009207	5’-GCCTTTGCGCATGGTGGTACT-3’ 5’-TGCCTCTGGACAGCAGCTACA-3’
Gapdh	NM_008084	5’-CCAATGTGTCCGTCGTGGAT-3’ 5’-TGCCTGCTTCACCACCTTCT-3’

Table S2. Primers for analyzing the transgene expression levels. Related to Experimental procedures.

Gene Name	Primer sequences
exo-Foxa3	5’-GTGGTACCTCACCCTTACCG-3’ 5’-TGGTGGGCACAGGATTCACT-3’
exo-Hnf1a	5’-GTGGTACCTCACCCTTACCG-3’ 5’-AGGCCTGGATCAGCACTTCC-3’
exo-Hnf1b	5’-GTGGTACCTCACCCTTACCG-3’ 5’-AGGCCTGGATCAGCACTTCC-3’

Supplemental Experimental Procedures

Generation of iHepSCs

To generate mouse iHepSCs, fibroblasts (5×10^4 cells) were infected with pMX retrovirus expressing the transcription factors in different combinations for 48 h. Prior to fibroblast transduction, the viral particles were produced for 48 h after transfecting 293T cells using a single pMX retroviral vector coding for one gene, together with the packaging plasmid pCL-Eco as previously described (Han et al., 2011; Han et al., 2012; Lim et al., 2016). The viral batches that showed transduction efficiency greater than 80% using the control GFP retrovirus were first transduced to generate iHepSCs. The cells transduced with different combinations of factors were cultured in hepatic stem cell culture medium (HepSCM): DMEM/F-12 supplemented with 10% fetal bovine serum (FBS; Hyclone), 0.1 μM dexamethasone (Sigma), 10 mM nicotinamide (Sigma), 1% ITS (insulin-transferrin-selenium) premix (Gibco), 1X penicillin/streptomycin/glutamine (Invitrogen), and hepatocyte growth factor (HGF; Peprotech), and epidermal growth factor (EGF; Peprotech) each at a final concentration of 10 ng/ml on gelatin-coated dishes. 20 nM DAPT (N-[N-(3,5-Difluorophenacetyl)-L-alanyl]-S-phenylglycine t-butyl ester, a γ-secretase inhibitor; Sigma), was added to HepSCM to block Notch signaling during cell culture.

***In vitro* differentiation**

For the hepatic differentiation of iHepSCs, we employed a previously described procedure (Li et al., 2006). Briefly, Matrigel (BD Bioscience) was added onto 6-well plate dishes (SPL) and solidified at 37°C for 30 min. 1×10^5 of iHepSCs were plated on Matrigel-coated dishes with hepatic differentiation medium (HDM): DMEM/F12 basal medium supplemented with 10% FBS (Hyclone), 20 ng/ml Oncostatin M (OSM; Peprotech), 20 ng/ml EGF (Peprotech), 0.1 μM dexamethasone, and 10 mM nicotinamide. Differentiation was induced for 7 days and HDM was changed every 2 days.

For the differentiation of iHepSCs into cholangiocytes, we used a 3D culture system as previously described (Li et al., 2010; Tanimizu et al., 2007). To induce branch structure formation during the differentiation of iHepSCs into cholangiocytes (Li et al., 2010), a mixture composed of 800 μl of 1.2 mg/ml type 1 collagen (Corning), 100 μl of 10× DPBS, 20 μl of 1N NaOH, and 80 μl of pure water carefully mixed on ice was used. To achieve differentiation into a cyst form (Tanimizu et al., 2007), a

mixture of 1.2 mg/ml Type 1 collagen and 40% Matrigel in 1:1 ratio (*v*/*v*) was itself mixed with an equal volume of 1×10^5 iHepSCs in cholangiocyte differentiation medium (CDM): DMEM/F12 basal medium supplemented with 10% FBS (HyClone) and 20 ng/ml HGF (Peprotech). Next, the cells in the mixture were transferred into 4-well plates, the mixture was left to solidify at 37°C for 30 min, and then fresh CDM was gently added onto the gel.

***In vitro* functional analyses of iHepSC-derived hepatocytes**

Periodic acid-Schiff (PAS or Schiff's reagent, Sigma) staining was performed following the manufacturer's instructions. Briefly, cells were fixed with 10% formalin in 95% cold ethanol and rinsed for 1 min with slowly running tap water, and then exposed to periodic acid solution for 5 min at room temperature. After rinsing several times with distilled water, cells were treated with Schiff's reagent for 15 min at room temperature, and then washed with tap water for 5 min.

For the indocyanine green (ICG, Sigma) uptake assay, ICG solution was added to the cultured cells at a final concentration of 1 mg/ml. The cells were incubated for 1 h at 37°C, washed three times with PBS, and then the cellular uptake of ICG was examined. For inducing the cellular release of ICG, cells were incubated in culture medium without ICG solution for 6 h at 37°C.

To assess the expression levels of Cyp450 enzymes, the cells were cultured in HDM supplemented with 50 μM 3-methylcholanthren (for *Cyp1a2*, *Cyp3a11*, *Cyp3a13*, and *Cyp3a44*), 25 μM rifampicin (for *Cyp2a5*), or 100 μM dexamethasone (for *Cyp2d22*) for 48 h at 37°C, and the expression levels were analyzed by qPCR.

To measure the amounts of mouse albumin in the culture medium, the cells were cultured for 48 h. To measure the amount of urea in the culture medium, 1 mM ammonium chloride (Sigma) was added in the culture medium. Mouse albumin and urea were detected using a Mouse Albumin ELISA Kit (Shibayagi) and QuantiChrom Urea Assay Kit (BioAssay Systems), respectively, according to the manufacturers' protocols.

***In vitro* functional analyses of iHepSC- or iCPC-derived cholangiocytes**

1 $\times 10^5$ of iHepSCs or iCPCs were differentiated into cholangiocytes for 7 days under the 3D culture condition as mentioned above. To assess MDR1 transporter activity in the cholangiocytes, the efflux of rhodamine 123 (Rho123; Molecular Probe) was evaluated by incubating iHepSC- or iCPC-derived cysts in culture medium containing 100 μM of Rho123 for 10 min. To test the effect of MDR1 inhibition, the culture medium was pretreated with 10 μM of verapamil (Ver; Sigma) for 30 min prior to treatment with Rho123. After washing the gels three times with the fresh medium, the number of cysts transporting Rho123 was counted under a fluorescence microscope.

To monitor the CFTR-mediated fluid transport and cyst swelling in the cholangiocytes, a forskolin-induced swelling assay was performed. The cysts were incubated in culture medium containing 10 μM calcein-AM (Thermo Fisher Scientific) for 30 min. Then, the gels were washed with fresh medium, and the cysts (at 0 h) were imaged under a fluorescence microscope. To stimulate the CFTR-mediated fluid transport and cyst swelling, the cysts were treated with 10 μM forskolin (FSK, a cAMP agonist; Enzo Life Sciences) and 100 μM IBMX (3-isobutyl-1-methylxanthine, nonselective PDE inhibitor; Sigma) for 24 h. To inhibit CFTR activity, the cysts were pretreated with 30 μM $CFTR^{inh}$-172 (a CFTR inhibitor; Sigma) or DMSO control for 3 h prior to the stimulation. After 24 h of FSK/IBMX treatment, the cysts were stained again and imaged under a fluorescence microscope. The total area of single cysts was calculated using ImageJ (NIH ver. 1.50) and the degree of swelling after 24 h of stimulation was quantified based on the unstimulated cyst size.

Transplantation of iHepSCs or iCPCs into DDC-treated mice

C57Bl6/J mice (8–10 weeks) were fed a diet containing 0.1% DDC (*wt*/*wt*). After 5 days with the DDC diet, the mice were transplanted intrasplenically with 1 × 10^6 iHepSCs or iCPCs labeled with GFP and maintained on the same diet. Body weight was monitored every week post-transplantation. Recipient mice were sacrificed 4 weeks after transplantation. Three random serial sections from the left, middle, and right liver lobes were examined by immunohistochemistry to determine the donor cell repopulation.

Gene expression analysis

Total RNA was isolated using a Hybrid-R™ (GeneAll) and 1 μg of total RNA was transcribed into cDNA with Reverse Transcriptase (Applied Biosystems) according to the manufacturer's instructions.

Quantitative real-time PCR (qPCR) was performed with SYBR green PCR Master Mix (Applied Biosystems). Expression levels were normalized to *Gapdh* values and calibrated relative to appropriate control samples. All the qPCR experiments were performed on an ABI 7500 real-time PCR system (Applied Biosystems).

RNA sequencing analysis

Sequenced reads were mapped to UCSC mm10 *Mus musculus* genome using STAR 2.4.1c (Dobin et al., 2013) with default parameter setting. Normalized read count values RPKMs (reads per kilobase of transcript per million mapped reads) were calculated for each gene using featureCounts (Liao et al., 2014) and edgeR 3.16.4 (Robinson et al., 2010). We added pseudo-value 1 to all original RPKM scores to compute fold changes. Genes with more than 4-fold changes in RPKM between samples were selected as representing differentially expressed genes (DEGs). To identify biological functions enriched in DEGs, we conducted hypergeometric tests for gene ontology biological process (GO:BP) terms. We also conducted gene set enrichment analysis (GSEA) for GOBP terms (Subramanian et al., 2005). Genes were sorted by their fold changes. We conducted GSEA-preranked with default parameters. A transcriptional regulatory network (TRN) was derived from CellNet (Cahan et al., 2014) by filtering for DEGs between MEFs and LEPCs. Network visualization and cluster analysis were conducted by Cytoscape 3.3.0 (Shannon et al., 2003) and MCODE 1.4.1 (Bader and Hogue, 2003) with default parameter setting (Accession number: GSE97507).

Gene ontology (GO) enrichment analysis

The database for annotation, visualization, and integrated discovery (DAVID) tool was used to analyze significantly enriched GO terms (biological process, BP) with the threshold value of group membership counts being set at 2 and with the EASE score being set at 0.1. *P*-values of GO terms were calculated by Fisher's exact tests using EASE and corrected with the Benjamini method. The importance of annotation groups was described by –log (p-value).

Immunocytochemistry

For immunofluorescence staining, the cells were fixed with 4% paraformaldehyde (Sigma) for 20 min at room temperature and then blocked with DPBS (Hyclone) containing 0.3% Triton X-100 (Sigma) and

5 % FBS (Hyclone) for 2 h at room temperature. The cells were then incubated with primary antibodies overnight at 4ºC, washed three times with DPBS, and then incubated with the appropriate fluorescence-conjugated secondary antibody for 2 h at room temperature in the dark. Nuclei were stained with Hoechst33342 (Fluka). Cells were observed under a fluorescence microscope or a confocal laser scanning microscope (Fluoview FV1000-ASWv1.5; Tokyo, Japan). Primary antibodies used for immunofluorescence are as follows: rabbit anti-E-cadherin (Cell Signaling, 3195S, 1:200); mouse anti-alpha-fetoprotein (R&D Systems, MAB1368, 1:100); mouse anti-Albumin (R&D Systems, MAB1455, 1:100); mouse anti-HNF4A (Abcam, ab41898, 1:100); mouse anti-CK7 (Abcam, ab9021, 1:200); rabbit anti-CK19 (Abcam, ab52625, 1:250); goat anti-EPCAM (Santa Cruz, SC23788, 1:100); rabbit anti-LGR5 (Abcam, ab75732, 1:200); rabbit anti-SOX9 (Novus Biologicals, NBP1-85551, 1:200); mouse anti-TROP2 (Santa Cruz, SC376181, 1:200); mouse anti-F-actin (Abcam, ab205, 1:200); and rabbit anti-ZO-1 (Invitrogen, 40-2200, 1:200).

Flow cytometric analysis

For flow cytometry analysis, the cells were fixed with 4% paraformaldehyde (Sigma) for 20 min and then permeabilized with 0.3% Triton X-100 (Sigma) for 10 min at room temperature. After blocking with 0.3% bovine serum albumin (Sigma) for 15 min, the cells were incubated with EPCAM or E-cadherin antibody for 30 min at 4°C. Cells were then incubated with secondary antibody for 20 min in the dark at 4°C. Cells were washed twice with DPBS containing 0.1% Tween20 (Sigma) and then analyzed by Calibur Flow Cytometer (Becton Dickinson). Primary antibodies used for the flow cytometry analyses are as follows: rabbit anti-E-cadherin (Cell Signaling, 3195S, 1:200) and rat anti-EPCAM (e-bioscience, 14-5791-81, 1:50). Untransduced MEFs were used as a negative control. Data were analyzed using FlowJo software (Tree Star).

Immunohistochemistry

Liver tissue samples were fixed overnight in 4% neutral buffered paraformaldehyde (Solarbio), embedded in paraffin, cut into 3-μm thick sections, and placed on adhesion microscope slides. For immunohistochemistry, deparaffinized and rehydrated slides were subjected to autoclave antigen retrieval in a 10 mmol/L citric acid buffer (pH 6.0) and allowed to cool to room temperature. Slides were blocked with 3% H_2O_2 for 15 minutes, washed in phosphate-buffered saline, and then blocked with 5%

normal horse serum in PBS. Slides were incubated with diluted primary antibodies overnight at 4°C. The following primary antibodies were used: mouse anti-GFP (Santa Cruz, SC9996, 1:200); rabbit anti-CK19 (Abcam, ab52625, 1:100); and rabbit anti-OPN (Millipore, AB1870, 1:1000). Secondary antibodies were used according to Vectastain ABC kits (Vector Laboratories), followed by DAB staining (DAKO).

Statistical analysis

Data are reported as mean values from at least three replicates, with error bars denoting standard deviation. Statistical significance was evaluated with unpaired two-tailed Student's *t*-test and/or paired *t*-test. Statistical analysis between diverse groups was conducted with one-way or two-way ANOVA using GraphPad Prism software.

Supplemental References

Bader, G.D., and Hogue, C.W. (2003). An automated method for finding molecular complexes in large protein interaction networks. BMC Bioinformatics *4*, 2.

Cahan, P., Li, H., Morris, S.A., Lummertz da Rocha, E., Daley, G.Q., and Collins, J.J. (2014). CellNet: network biology applied to stem cell engineering. Cell *158*, 903-915.

Dobin, A., Davis, C.A., Schlesinger, F., Drenkow, J., Zaleski, C., Jha, S., Batut, P., Chaisson, M., and Gingeras, T.R. (2013). STAR: ultrafast universal RNA-seq aligner. Bioinformatics *29*, 15-21.

Han, D.W., Greber, B., Wu, G., Tapia, N., Arauzo-Bravo, M.J., Ko, K., Bernemann, C., Stehling, M., and Scholer, H.R. (2011). Direct reprogramming of fibroblasts into epiblast stem cells. Nat Cell Biol *13*, 66-71.

Han, D.W., Tapia, N., Hermann, A., Hemmer, K., Hoing, S., Arauzo-Bravo, M.J., Zaehres, H., Wu, G., Frank, S., Moritz, S., *et al.* (2012). Direct reprogramming of fibroblasts into neural stem cells by defined factors. Cell Stem Cell *10*, 465-472.

Li, F., Liu, P., Liu, C., Xiang, D., Deng, L., Li, W., Wangensteen, K., Song, J., Ma, Y., Hui, L., *et al.* (2010). Hepatoblast-like progenitor cells derived from embryonic stem cells can repopulate livers of mice. Gastroenterology *139*, 2158-2169 e2158.

Li, W.L., Su, J., Yao, Y.C., Tao, X.R., Yan, Y.B., Yu, H.Y., Wang, X.M., Li, J.X., Yang, Y.J., Lau, J.T., *et al.* (2006). Isolation and characterization of bipotent liver progenitor cells from adult mouse. Stem Cells *24*, 322-332.

Liao, Y., Smyth, G.K., and Shi, W. (2014). featureCounts: an efficient general purpose program for assigning sequence reads to genomic features. Bioinformatics *30*, 923-930.

Lim, K.T., Lee, S.C., Gao, Y., Kim, K.P., Song, G., An, S.Y., Adachi, K., Jang, Y.J., Kim, J., Oh, K.J., *et al.* (2016). Small Molecules Facilitate Single Factor-Mediated Hepatic Reprogramming. Cell Rep.

Robinson, M.D., McCarthy, D.J., and Smyth, G.K. (2010). edgeR: a Bioconductor package for differential expression analysis of digital gene expression data. Bioinformatics *26*, 139-140.

Shannon, P., Markiel, A., Ozier, O., Baliga, N.S., Wang, J.T., Ramage, D., Amin, N., Schwikowski, B., and Ideker, T. (2003). Cytoscape: a software environment for integrated models of biomolecular interaction networks. Genome Res *13*, 2498-2504.

Subramanian, A., Tamayo, P., Mootha, V.K., Mukherjee, S., Ebert, B.L., Gillette, M.A., Paulovich, A., Pomeroy, S.L., Golub, T.R., Lander, E.S., *et al.* (2005). Gene set enrichment analysis: a knowledge-based approach for interpreting genome-wide expression profiles. Proc Natl Acad Sci U S A *102*, 15545-15550.

Tanimizu, N., Miyajima, A., and Mostov, K.E. (2007). Liver progenitor cells develop cholangiocyte-type epithelial polarity in three-dimensional culture. Mol Biol Cell *18*, 1472-1479.